Deletion of the Parathyroid Hormone Receptor in Marrow Adipose Lineage Precursors (MALPs) Prevents Their Negative Regulation of Skeletal Homeostasis

A Thesis Presented by

Lama Abdulrahman I Alabdulaaly

to

The Faculty of Medicine

In partial fulfillment of the requirements

for the degree of

Doctor of Medical Science

Research Mentors:

Roland Baron

Professor and Chair of Oral Medicine, Infection, and Immunity

Harvard School of Dental Medicine

Boston, Massachusetts

Francesca Gori

Assistant Professor of Oral Medicine, Infection, and Immunity

Harvard School of Dental Medicine

Boston, Massachusetts

April 2021

Acknowledgements

Foremost, I thank the Almighty Allah for the strength, health, and blessings bestowed on me.

It is my privilege to extend my utmost gratitude to my beloved mother Dr. Huda Alabdulaaly for being the family's pillar of strength and my idol, to my father Dr. Abdulrahman Alabdulaaly, for his lifelong infinite support and confidence in me, and to my late grandmother, Loloah, for being the source of grit during my educational journey. I would like to thank my sister Maram, for her continuous encouragement and advice. It is my pleasure to express my gratefulness to my brothers Ibrahim, Fahad, and Abdullah.

I would like to express my deepest appreciation to my exceptional mentors, Dr. Roland Baron and Dr. Francesca Gori. Throughout the years, their continuous and generous guidance refined my skills, and their inspiration prospered my passion towards basic science research. I am greatly beholden to them for having a pivotal role in shaping my career path.

It is my pleasure to acknowledge Dorothy Hu, Shawn Berry, Noriko Ide, Alann Thaffarell, and the members of Baron-Gori laboratory for their indispensable assistance.

I would like to extend my appreciation to the thesis advisory and defense committees, Dr. Clifford Rosen, Dr. Beate Lanske, Dr. Bjorn Olsen, Dr. Herve Sroussi, and Dr. Corneliu Sima, for taking the time to review the thesis and provide valuable insights.

I would like to express my gratitude to my program director Dr. Sook-Bin Woo, and my colleagues in the Oral Pathology and Oral Medicine programs.

I extend my gratitude to my sponsor King Saud bin Abdulaziz University for Health Sciences for providing me with scholarship and financial assistance throughout this journey.

This research is supported by NIH grants R01 DK112374 and R01 AR073774 to C.R and R.B. We thank the Harvard Neurobiology Imaging Facility (supported by P30 grant #2P30NS072030) for their services and the Brigham and Women's Hospital Human Immunology Center Flow Core for their assistance with cell sorting.

Deletion of the Parathyroid Hormone Receptor in Marrow Adipose Lineage Precursors (MALPs) Prevents Their Negative Regulation of Skeletal Homeostasis

Abstract

Background and objectives: Parathyroid hormone (PTH) is essential for skeletal homeostasis and PTH[1-34] (teriparatide) is used to treat severe osteoporosis, medication-related osteonecrosis of the jaws, and enhance implant osseointegration. PTH exerts its anabolic actions by acting on osteoblasts, bone lining cells, and osteocytes. Recently, marrow adipose lineage precursors (MALPs) have been reported to suppress osteogenesis and enhance osteoclastogenesis. We hypothesized that, since MALPs express the PTH receptor 1 (*Pth1r*), they may contribute to the skeletal response to PTH.

Methods: We deleted *Pth1r* specifically in MALPs and their lineage (adipocytes) using *Adiponectin Cre* (*AdipoqCre*) and *tdTomato* was used as a reporter. *AdipoqCre;Pth1r*$^{fl/fl}$*,tdTomato*$^{fl/fl}$ mice (*Pth1r*^{MALPs}) were used as experimental mice and age- and sex-matched *AdipoqCre;Pth1r*$^{fl/fl}$*,tdTomato*$^{fl/fl}$ and *Pth1r*$^{fl/fl}$*,tdTomato*$^{fl/fl}$ were used as controls. The skeletal phenotype was characterized by microscopic computed tomography (μCT) and dynamic histomorphometry at 4, 7, and 12 weeks of age. Bone marrow adipose tissue (BMAT) was assessed by osmium tetroxide staining and μCT analysis. The proximal one-third of the tibiae was designated as regulated BMAT (rBMAT) and the distal one-third was designated as constitutive BMAT (cBMAT).

Colony forming unit (CFU) assays, flow cytometry, and fluorescence-activated cell sorting (FACS) were performed on flushed bone marrow stromal cells (BMSC). Two-way ANOVA and Student's t-test were used for statistical analysis ($\alpha = 0.05$).

Results: *Pth1r*^{MALPs} female mice exhibited a 54.2%, 15.8%, and 42.7% increase in trabecular bone volume at 4, 7, and 12 weeks of age, respectively ($p = 0.001$). The increase in bone volume was associated with a significant increase in labeled surfaces (MS/BS and dLS/BS, $p = 0.0066$ and $p = 0.0429$, respectively by two-way ANOVA) but an increase in bone formation rate (BFR/BS) was significant only at 4 weeks of age ($p = 0.03$). Flow cytometry analysis revealed that osteochondrogenic progenitor cells were decreased by half in *Pth1r*^{MALPs} mice ($p = 0.01$). Since mineralizing surfaces were increased, these results suggest a shift of the progenitor pool towards differentiated and functional osteoblasts. Additionally, the number of CFU-F colonies was significantly decreased in *Pth1r*^{MALPs} cells, further confirming the decrease in the progenitors. In contrast, the CFU-Ob remained similar between the two groups, suggesting an increase in the osteogenic potential of cells from *Pth1r*^{MALPs} mice despite their decreased number. Only 6.4% ± 4.6% of CFU-Ob cells represented a distinct population of *tdTomato*+ cells, and 5.7% ± 2.7% had a dim *tdTomato*+ signal (herein, *tdTomato*+ dim). Interestingly, cells from *Pth1r*^{MALPs} mice exhibited an 8-fold increase in *tdTomato*+ dim cells, and unfractionated CFU-Ob cells exhibited a 90.3% decrease in *Pth1r* mRNA gene expression ($p = 0.001$). Additionally, *Pth1r*^{MALPs} mice showed a significantly higher rBMAT density, confirming that PTH suppresses adipogenesis. Importantly, sorted MALPs expressed *Rankl*, and its expression is increased in MALPs lacking *Pth1r*. The

endosteal osteoclast number and surface was increased in *Pth1r*^{MALPs} mice, indicating that PTH signaling in MALPs suppress osteoclastogenesis.

Conclusions: Deletion of the *Pth1r* in MALPs partially prevents their suppression of osteogenesis through driving the progenitor pool to a differentiated state. Moreover, PTH signaling in MALPs suppresses adipogenesis and osteoclastogenesis.

Graphical abstract

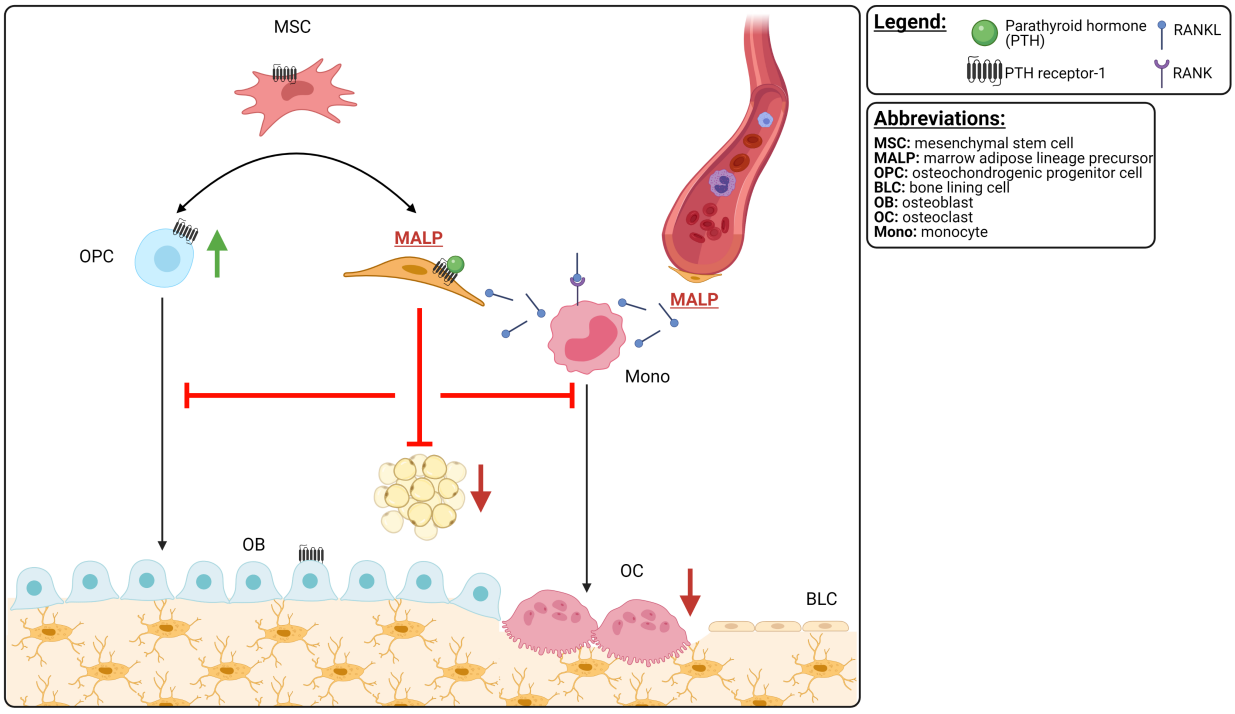

Introduction

The bone marrow is a highly orchestrated environment that has long been recognized for its essential role in hematopoiesis. Until recently, and with the advent of advanced lineage tracing technologies, the bone marrow stem/stromal cell (BMSC) has gained considerable interest. At the single cell level, the non-hematopoietic bone marrow is composed of at least 17 cell populations (Baryawno et al., 2019, Tikhonova et al., 2019, Wolock et al., 2019, Zhong et al., 2020, Baccin et al., 2020, Matsushita et al., 2020). In addition to single cell RNA sequencing (scRNA-seq) models, various models have been proposed to segment the non-hematopoietic bone marrow compartment by surface marker profiling (Chan et al., 2015, Ambrosi et al., 2017, Ambrosi et al., 2019, Kurenkova et al., 2020). Common to the conclusions reached by all of the aforementioned models, regardless of the markers and methods utilized, is the presence of (i) a mesenchymal stromal cell (MSC) with multipotency and self-renewal capabilities, (ii) an osteoblastic lineage, (iii) a chondroblastic lineage, (iv) an adipocytic lineage, and (v) other populations (such as fibroblasts and endothelial cells) within the non-hematopoietic component of bone marrow. Recently, a novel BMSC population that expresses common stem cell markers and exists in a perivascular location has been described (Zhong et al., 2020). In addition to expressing stem cell markers, these cells lack lipid droplets while expressing adipocyte-specific genes (such as *Adiponectin* [*Adipoq*]), and, hence, were named ‘marrow adipose lineage precursors (MALPs)’ (Zhong et al., 2020).

MALPs are a major source of Receptor activator of nuclear factor kappa-B ligand (RANKL) production, a key ligand that induces osteoclastic differentiation and bone

resorption (Yu et al., 2020). In addition, they suppress osteogenesis (Zhong et al., 2020, Zou et al., 2020), play a role in type H endothelium-lined blood vessel (THEC) maintenance (Zhong et al., 2020), participate in restoring the bone marrow cells following radiation and chemotherapy (5-fluorouracil), and play an integral role in secreting stem cell factor (SCF) protein essential for the regeneration of the hematopoietic stem cell (HSC) niche (Zhou et al., 2017).

The parathyroid hormone (PTH) signaling pathway is fundamental to many organ systems, and in particular the bone and the kidney, where it regulates calcium and phosphate metabolism. PTH is a key regulator of skeletal homeostasis and a bioactive form of this hormone (PTH[1-34], teriparatide) is one of the few anabolic treatments approved for use in severe osteoporosis (Neer et al., 2001, Black and Rosen, 2016). PTH exerts its actions on many cell types, including bone lining cells, osteoblasts, and osteocytes (Wein and Kronenberg, 2018). Importantly, it has also been shown to affect BMSCs and their potential to differentiate into osteogenic or adipogenic cells (Fan et al., 2017). In the osteoblastic lineage, the PTH receptor (*Pth1r*) is necessary for trabecular bone maintenance. Our group has previously showed that lack of *Pth1r* in *Paired-Related Homeobox 1 (Prx1)*-expressing mesenchymal progenitors in the appendicular skeleton leads to a dramatic decrease in trabecular and cortical bone mass, disruption of the growth plate, in addition to an increase in bone marrow adipose tissue (BMAT) (Fan et al., 2017). However, *Prx1* is expressed in many cell types in the bone marrow including early progenitors as well as osteoblasts, chondrocytes, and MALPs (GSE145477 from (Zhong et al., 2020)). The specific role of *Pth1r* in MALPs has not yet been explored. Ablation of these cells using the *Adipoq Cre* promoter and the Diphtheria

toxin receptor (DTR) method results in a marked increase in bone mass (Zou et al., 2020). Depletion of *Rankl* from MALPs produces a similar high bone mass phenotype (Yu et al., 2020). This suggests that the increase in bone mass seen in these models is mainly due to a decrease in bone resorption, and not only that MALPs can secrete RANKL locally but also that they are an important source of this osteoclastogenic cytokine.

Since MALPs express *Pth1r* (GSE145477 from (Zhong et al., 2020)), we asked whether PTH signaling in MALPs regulates osteogenesis, osteoclastogenesis, and adipogenesis. To address this question, we generated a mouse model that conditionally deletes *Pth1r* in MALPs using *AdipoqCre,* which was shown to efficiently recombine in MALPs and lipid-laden adipocytes (LiLa), with limited recombination in osteoblasts and chondrocytes (Yu et al., 2020). We show that PTH signaling in MALPs surprisingly contributes to the MALP-induced suppression of osteogenesis and osteoclastogenesis evidenced by the increase in trabecular bone mass in adult mice upon *Pth1r* deletion in MALPs. Furthermore, we report that *Pth1r* in MALPs impairs the differentiation of osteochondroprogenitor cells into well-differentiated osteoblasts. Lastly, we show for the first time that PTH signaling in MALPs suppresses adipogenesis.

Results

Adiponectin Cre recombines in adipose lineage in the marrow and peripheral adipose tissue

To generate a conditional mouse model where *Pth1r* is deleted in adipose lineage including MALPs and which allows tracing of the cell lineage, we crossed

AdipoqCre;tdTomato$^{fl/fl}$ male mice with floxed *Pth1r* female mice as described previously (Kir et al., 2016, Fan et al., 2017). To verify the *AdipoqCre* specific recombination in adipose tissue, we used the red florescent protein *tdTomato* to visualize sites of *Adiponectin* expression following *Cre* recombination. Whole body fluorescence imaging showed *tdTomato* expression in peripheral adipose tissue of *AdipoqCre;Pth1r*$^{fl/fl}$*,tdTomato*$^{fl/fl}$ (herein referred to as *Pth1r*^{MALPs}) while *Pth1r*$^{fl/fl}$*,tdTomato*$^{fl/fl}$ mice (herein referred to as control) lacked *TdTomato* expression (**Figure S1A**). Macroscopic images of peripheral adipose tissue harvested from interscapular brown adipose tissue (iBAT), inguinal white adipose tissue (iWAT) and epididymal white adipose tissue (eWAT) confirmed the *tdTomato* expression in *AdipoqCre;tdTomato*$^{fl/fl}$ mice (**Figure S1B**). The kidney was used as an internal control and, as expected, lacked *tdTomato* expression, while peri-renal fat expressed *tdTomato*. Consistently, mice lacking *AdipoqCre* lacked *tdTomato* expression in all tissues examined. Gene expression analysis showed efficient and significant (95%) deletion of *Pth1r* in iWAT (**Figure S1C**). These results confirmed that *AdipoqCre* targets the adipose lineage.

To test whether MALPs express *Pth1r*, we flushed bone marrow cells and sorted the CD31-/CD45-/Ter119-/*tdTomato*+ cells (MALPs) and CD31-/CD45-/Ter119-/*tdTomato*- cells (**Figure S1D**). Compared to *tdTomato*- cells, MALPs showed a 16-fold increase in *Pth1r* expression in the control mice (**Figure S1E**). MALPs from *Pth1r*^{MALPs} mice exhibited a 50% decrease in *Pth1r* expression, confirming that *AdipoqCre* targets MALPs (**Figure S1E**).

PTH signaling in MALPs contributes to their suppression of osteogenesis via blocking the differentiation of the osteochondroprogenitor niche

Since MALPs suppress osteogenesis (Zou et al., 2020, Zhong et al., 2020), we speculated that this osteogenesis inhibition could be regulated by PTH signaling. To test this hypothesis, we analyzed the skeletal phenotype of mice at 4, 7, and 12 weeks of age by microscopic computed tomography (μCT). Two-way ANOVA showed that there was a strong effect of the deletion on several structural parameters and in particular BV/TV was significantly (p = 0.001) increased in the *Pth1r*^{MALPs} female mice. *Pth1r*^{MALPs} mice exhibited an increase in trabecular bone volume by 54.2%, 15.8%, and 42.7% at 4, 7, and 12 weeks of age, respectively and two-way ANOVA also showed a strong effect of age (p = 0.0002) (**Figure 1A-B and supplementary table 1**). Male mice exhibited a similar trend but did not reach statistical significance (**Figure S2**). Given that the skeletal phenotype was more significant in females, we focused our experiments on female mice, henceforward.

Surprisingly, and despite the presence of a higher bone volume in 12-week-old mice, we have not been able to detect changes in bone formation rates. This suggested the possibility that changes occurred at earlier time points, leading to higher peak bone mass. As anticipated, bone formation rate/bone surface (BFR/BS), mineralizing surface (MS/BS), and osteoid thickness (O.Th) were increased in 4-week-old female mice (**Figure 1C-D**). This increase blunts at the peak bone mass age.

MALPs are located primarily within the medullary cavity with limited presence on the periosteal surface (**Figure 2A**) (Yu et al., 2020). Therefore, we did not expect to observe a skeletal phenotype in the cortical bone of *Pth1r*^{MALPs} mice. Consistent with

our expectations, cortical bone volume and thickness were similar between control and *Pth1r*^{MALPs} mice (**Figure 2B-C**).

MALPs ablation results in osteosclerosis associated with an expansion of the osteoblastic lineage (Zou et al., 2020). Cells that lack Stem cell antigen 1 (Sca1) and express Platelet derived growth factor-α (Pα) were found to be unilaterally committed osteochondrogenic progenitor cells (OPC; defined as CD31-/CD45-/Sca1-/Pα+), and capable of forming bone-like structure *in vivo* (Ambrosi et al., 2017). Given that *Pth1r*^{MALPs} mice exhibit an increase in trabecular bone mass and osteoid surface, we asked how OPC and multipotent stem cells (MSCs) contribute to the observed phenotype, and how PTH signaling in MALPs affects the differentiation fate of MSCs. While the MSC proportions remained similar between *Pth1r*^{MALPs} mice and littermate controls (**Figure 3A-B**), the OPC percentage was decreased by 50% in *Pth1r*^{MALPs} mice (p = 0.0116, **Figure 3C-D**). *Gremlin1* (*Grem1*) is a bone morphogenetic protein (BMP) antagonist that mediates, at least in part, MALPs-dependent suppression of osteogenesis (Zou et al., 2020). Additionally, *Grem1* marks osteochondroreticular (OCR) stem cells (Worthley et al., 2015). We analyzed *Grem1* gene expression from freshly sorted bone marrow cells and found that *Grem1* is expressed in MALPs at a higher level than *tdTomato-* cells. Consistent with the decrease in OPC cells, *Grem1* was decreased in *Pth1r*^{MALPs} mice by 80%, further confirming the decrease in osteogenic progenitors (**Figure 3E**). We wondered how this decrease in progenitors reflects on the number of well-differentiated osteoblasts. We used *Osterix (Osx)* to label well-differentiated osteoblasts and found that the number of *Osx*+ cells mildly increased upon deletion of *Pth1r* MALPs (**Figure 3F**). Consistent with previous reports (Zhong et

al., 2020), the majority of *Osx*+ cells were *tdTomato*- (**Figure 3F**). Taken together, these data suggest that PTH signaling in MALPs suppresses osteogenesis by maintaining the OPC pool by inhibiting their differentiation into osteoblasts.

Given that *Pth1r*^{MALPs} mice exhibit a decrease in the OPC population, which are reported to have high CFU-F potential (Morikawa et al., 2009, Ambrosi et al., 2017), we wondered how this decrease in OPCs affects CFU-F formation. Although MALPs do not contribute to colony forming unit-fibroblast (CFU-F) formation (Zhong et al., 2020, Yu et al., 2020), ablation of MALPs decreases CFU-F colonies (Zhong et al., 2020), suggesting that MALPs have the ability to act on bone marrow progenitors in a paracrine manner, at least *ex vivo*. Cells from *Pth1r*^{MALPs} mice exhibited a significant decrease in CFU-F colonies (**Figure 4A-B**). To quantify the percentage of MALPs within CFU-F colonies, we performed flow cytometry analysis of CFU-F cells after 10 days of culture (**Figure 3C**). The *tdTomato*+ cells represented only 2.1 ± 2.4% of the CFU-F cells. However, we noted an intermediate cell population that we labelled as '*tdTomato*+ dim', and these represented 2.47 ± 1.9% of the CFU-F cells (**Figure 4D-E**). Collectively, *tdTomato*+ bright and *tdTomato*+ dim add up to 4.6 ± 3.1% of CFU-F cells. On the other hand, cells from *Pth1r*^{MALPs} mice have a significantly higher percentage of total *tdTomato*+ cells (bright and dim) in CFU-F colonies (**Figure 4E**). Collectively, the low *tdTomato* positivity in the CFU-F cells and the associated decrease in colonies upon *Pth1r* ablation from MALPs confirm MALPs' ability to act upon bone marrow progenitors.

MALPs do not form bone-like structures *in vivo* (Zhong et al., 2020). Although we did not observe changes in CFU-osteoblast (CFU-Ob, **Figure 4F-G**), the ratio of CFU-Ob to CFU-F was significantly increased (**Figure 4H**), further confirming a shift towards the

osteogenic lineage upon *Pth1r* deletion in MALPs. In addition, CFU-Ob cells exhibited an increase in osteoblast differentiation genes (**Figure 4I**), suggesting that the decrease in progenitors is caused by a shift towards a more differentiated state. Only a low percentage of CFU-Ob cells were *tdTomato*+ bright cells (6.3 ± 4.6%), with no difference between cells from the control mice and $Pth1r^{MALPs}$ mice. Of note, CFU-Ob cells from $Pth1r^{MALPs}$ mice had an 8-fold increase in the percentage of *tdTomato*+ dim cells (**Figure 4-KJ**). Interestingly, unfractionated CFU-Ob cells exhibited a 90.3% decrease in *Pth1r* mRNA gene expression ($p = 0.0014$, **Figure 4L**) suggesting that the *Adipoq Cre* had been sufficiently activated at some point in the differentiation of these cells to delete the *Pth1r*.

PTH signaling in MALPs suppresses adipogenesis

Osteoporosis is associated with increased bone marrow adipogenesis (Veldhuis-Vlug and Rosen, 2018), and PTH administration decreases marrow adipogenesis (Turner and Iwaniec, 2011, Yang et al., 2016, Fan et al., 2017). PTH plays a role in BMSC fate decision by favoring osteogenesis and suppressing adipogenesis (Fan et al., 2017). Given that MALPs differentiate from a *Prx1*-expressing progenitor, we hypothesized that *Pth1r* deletion in MALPs would result in a similar phenotype to the $Prx1Cre;Pth1r^{fl/fl}$ mice. Thus, we sought to examine the effects of MALP-specific PTH signaling on adipogenic progenitors (APC) and well-differentiated (i.e. lipid-laden) adipocytes (LiLA). APCs are CD31-/CD45-/Sca1+/CD24- (Ambrosi et al., 2017), and $Pth1r^{MALPs}$ mice exhibited a 28% non-significant increase in APCs compared to littermate controls (**Figure 5A-B**). We then examined the effects of the APC increase on lipid-laden

adipose tissue by osmium tetroxide staining followed by μCT analysis. While BMAT volume and density remained unchanged at 4 weeks of age, 7-week-old *Pth1r*^{MALPs} mice exhibited a significant increase in regulated BMAT (rBMAT) volume and density, whereas constitutive BMAT (cBMAT) remained unchanged (**Figure 5C-D and supplementary table 2**). To assess the adipogenic differentiation potentials *ex vivo*, we cultured flushed unfractionated/whole bone marrow (WBM) under adipogenic conditions to assess CFU-adipocyte (CFU-Ad) formation capabilities. Cells from *Pth1r*^{MALPs} mice and littermate controls exhibited a comparable CFU-Ad/CFU-F ratio (**Figure 5E**). As expected, the majority of CFU-Ad cells were *tdTomato*+ (**Figure 5F**). These results establish that PTH signaling in MALPs contributes to the suppression of adipogenesis.

PTH signaling in MALPs suppresses *Rankl* expression and osteoclastogenesis

It is well established that PTH increases RANKL production from the osteoblast lineage (Huang et al., 2004, Xiong et al., 2014). However, it was recently shown that MALPs are also a major source of RANKL production (Yu et al., 2020), and we previously showed that *Rankl* gene expression from BMSC as well as BMAT increases upon ablation of *Pth1r* in *Prx1*-expressing cells (Fan et al., 2017). Therefore, we expected that deletion of *Pth1r* in MALPs would increase *Rankl* expression and osteoclast differentiation. As expected, *Rankl* expression was higher in freshly sorted MALPs compared to *tdTomato*- cells (**Figure 6A**). In addition, MALPs exhibited a 7-fold increase in *Rankl* expression upon *Pth1r* deletion (**Figure 6A**). We then quantified tartrate-resistant acid phosphatase (TRAP)-positive cells at 4, 7, and 12 weeks of age. Endosteal osteoclast number was increased by 18.2%, 72.0%, and 49.9% in 4-, 7-, and 12-week-old *Pth1r*^{MALPs} mice,

respectively (**Figure 6B-C and supplementary table 3**). A similar trend was observed in trabecular bone, albeit not reaching statistical significance (**Figure 6D-E and supplementary table 3**). These results suggest that, while PTH signaling in the osteoblast lineage increases osteoclastogenesis, PTH signaling in the adipose lineage suppresses osteoclastogenesis, providing a dampening mechanism.

We next analyzed serum biomarkers of bone resorption, C-terminal telopeptide of type I collagen (CTX-I), and bone formation, N-terminal propeptide of type I procollagen (PINP). Changes in CTX-I and PINP were not detected (**Figure 6F**). These results indicate that the skeletal phenotype is not substantial enough to result in a change in serum biomarkers.

Pth1r deletion in adipose tissue does not alter peripheral adipose tissue

Given that both *Adiponectin* and *Pth1r* are expressed in other organ systems outside of the bone marrow, including peripheral adipose tissues where *Pth1r* is deleted in our model, we were concerned that a change in energy metabolism may have an effect on the skeletal phenotype observed in $Pth1r^{MALPs}$ mice rather than a process exclusive to the bone marrow adipose lineage. Consistent with previous results (Kir et al., 2016), we did not observe any changes in body weights and adipose tissue weights nor did we observe any microscopic changes in brown and white adipocytes size (**Figure S3**). Kir et al (Kir et al., 2016) studied the *AdipoqCre;*$Pth1r^{fl/fl}$ mice in the context of energy metabolism prior to the description of MALPs, and did not detect any changes in energy metabolism upon deletion of *Pth1r* in the adipose lineage. Thus, these findings demonstrate that *Pth1r* ablation in adipose tissue is not altering fat depots other than

BMAT and, therefore, loss of PTH signaling in these fat depots does not contribute significantly to the bone phenotype, suggesting that the regulation of skeletal homeostasis through *Pth1r* signaling in MALPs is cell autonomous.

PTH signaling in MALPs is not critical for type H endothelial cell and hematopoietic stem cell maintenance

Type H endothelial cells (THEC, defined as Endomucin [Emcn]^{hi}/CD31^{hi}) are found exclusively in the bone marrow, and are intimately associated with osteoprogenitor cells (Kusumbe et al., 2014). Intermittent PTH treatment temporarily decreases THECs (Caire et al., 2019), and MALPs are necessary for the maintenance of THECs (Zhong et al., 2020). Given that *Pth1r*^{MALPs} mice exhibit a decrease in osteochondroprogenitors, we hypothesized that this decrease in osteochondroprogenitors is associated with a decrease in THECs. We quantified THECs from flushed bone marrow and did not observe any changes upon *Pth1r* deletion (**Figure 7A-B**). Therefore, PTH signaling does not appear to play a role in MALPs-dependent THEC maintenance, and MALPs may not participate in PTH-mediated suppression of THECs.

The bone marrow hematopoietic and mesenchymal compartments are known to interact in physiologic and pathologic states (Omatsu et al., 2010, Fairfield et al., 2016, McDonald et al., 2017), and PTH administration expands the HSC compartment and improves HSC survival following chemotherapy (Calvi et al., 2003, Adams et al., 2007). *Scf*, a cytokine necessary for HSC maintenance (Ding et al., 2012), is expressed in *Adipoq*+ cells (Ding and Morrison, 2013, Zhou et al., 2017). Ablation of *Scf* from *AdipoqCreER*+ cells prevents the partial recovery of HSC following radiation and

chemotherapy (Zhou et al., 2017). While the detailed investigation of the MALPs' role in the context of hematopoiesis is beyond the scope of this thesis, we sought to analyze the outcomes of absence of PTH signaling in MALPs on different hematopoietic cell populations. We quantified multipotent hematopoietic progenitors (MPP), hematopoietic progenitor cells-1/2 (HPC-1 and HPC-2), and HSC (Oguro et al., 2013). We did not detect any changes in the MPP, HSC, HPC-1, and HPC-2 percentages (**Figure 7C-D**). These data imply that PTH signaling in MALPs does not participate in their HSC maintenance.

Discussion

Using mouse genetics, we show that PTH signaling in MALPs contributes to their suppression of both osteogenesis and adipogenesis. PTH signaling in MALPs maintains the osteochondrogenic progenitor niche by suppressing their differentiation into osteoblasts. Similarly, we confirm that PTH signaling in MALPs suppresses adipogenesis. In addition, we further expand on the role of PTH signaling in MALPs on osteoclastogenesis. We confirmed that this regulation of skeletal homeostasis is mainly localized to the bone marrow, with limited changes in energy metabolism.

Osteoporosis, which affects 10% of women in their 6^{th} decade and its prevalence increases to 66% in women older than 90 years of age, is a metabolic bone condition associated with decreased bone mass, and, consequently, increased risk of fracture (Kanis et al., 2019, Johnston and Dagar, 2020). A few anabolic agents have been approved for the treatment of osteoporosis (Johnston and Dagar, 2020). One of the earliest anabolic medications used is the parathyroid hormone (1-34, teriparatide) (Neer

et al., 2001). A number of cell types respond to PTH within the bone marrow, including the BMSC, osteoblast, osteocyte, bone lining cell, and T lymphocytes. While the PTH effects *in vitro* were studied extensively (Wein and Kronenberg, 2018), *in vivo* actions of PTH are not fully understood. Analogous to the skeletal changes seen in Blomstrand chondrodysplasia (OMIM #215045), global lack of *Pth1r* results in premature mineralization of the growth plate and, consequently, shortening of the limbs (Lanske et al., 1996). Balani et al (Balani et al., 2017) demonstrated an expansion of the osteoblast lineage cells coupled with decreased apoptosis of these cells following teriparatide administration, and lack of the *Pth1r* receptor in *Sox9*-expressing cells prevented the increase in the osteoblast lineage cells (Balani et al., 2017). Lack of *Pth1r* in *Osteocalcin* (*Ocn)*+ cells results in kyphosis and shortened limbs (Qiu et al., 2015). Similarly, lack of PTH signaling in *Osx*+ cells results in shorter limbs (Sinha et al., 2014, Gardinier et al., 2019). Constitutive activation of *Pth1r* in *Col1*+ cells increases trabecular bone mass (Calvi et al., 2001). Taken together, these findings indicate that PTH signaling in early and late osteoblastic lineage is necessary to maintain the bone mass by reducing osteoblast apoptosis and increasing the differentiation of the early osteoblast lineage into osteoblasts. Contrary to these findings, When *Pth1r* is conditionally ablated from osteoblasts and osteocytes using the *Dentin matrix protein-1* (*Dmp1*) promoter, an increase in trabecular bone volume was observed, with no changes in cortical bone volume (Delgado-Calle et al., 2017).

In general, PTH signaling shifts the BMSC to the osteogenic lineage, while suppressing adipogenesis (Yu et al., 2012, Li et al., 2013, Fan et al., 2017). Li et al (Li et al., 2013) demonstrated an LRP6-dependent increase in *Ocn*+ cells following

intermittent PTH treatment. In addition, Yu et al (Yu et al., 2012) showed that short-term PTH treatment shifts Sca1+ MSCs to Osx+ cells. Therefore, and given the increase bone mass in *Pth1r*^{MALPs} mice, we hypothesized that *Pth1r* ablation from the adipogenic, not the osteogenic lineage or the MSCs, could expand the osteogenic lineage. Although we observed a decrease in OPC, we demonstrated an increase in osteoid thickness and mineralizing surface. Despite that *Pth1r*^{MALPs} mice had less CFU-F colonies, CFU-Ob differentiation was similar between *Pth1r*^{MALPs} mice and littermate controls, implying that progenitors from *Pth1r*^{MALPs} mice have an enhanced capability of osteoblastic differentiation albeit their decreased number. These results suggest that loss of PTH signaling in MALPs decreases the progenitor pool by shifting them into a more differentiated and functional states.

The majority of cells forming CFU-F colonies are non-MALPs. Zhong et al (Zhong et al., 2020) reported that only 2.03% of CFU-F cells were *tdTomato*+ by flow cytometry. Consistently, we showed that only 2.1 ± 2.4% of cells within the CFU-F colonies were *tdTomato*+ bright, while the remaining were *tdTomato*- and *tdTomato* dim (2.47 ± 1.94%). Since the majority of CFU-F cells are non-MALPs, it is counterintuitive that we observed a decrease in CFU-F formation. Indeed, when MALPs were ablated, Zhong et al observed a decrease in CFU-F colonies (Zhong et al., 2020), suggesting that MALPs exert paracrine effects on bone marrow progenitors.

In vivo, *AdipoqCre;tdTomato*+ cells do not form bone-like structures when transplanted under the renal capsule (Zhong et al., 2020). Yu et al (Yu et al., 2020) cultured *AdipoqCre;tdTomato*-negative cells under adipogenic and osteogenic conditions. Cells in adipogenic medium gained *tdTomato* expression, while cells in

osteogenic medium did not. We cultured WBM cells under osteogenic conditions, and 6.35 ± 4.6% and 5.72 ± 2.7% of cells in CFU-Ob colonies were *tdTomato*+ bright and *tdTomato*+ dim, respectively. One possible explanation for the presence of *tdTomato* dim signal is *Cre* mosaicism, a phenomenon observed with other *Cre* promoters (Heffner et al., 2012). Another plausible explanation is that these *tdTomato*+ dim cells are *tdTomato*- cells in the process of committing to the adipogenic lineage and gradually acquiring *Adipoq* expression. We believe that the latter explanation is more likely to be true. We supported this notion by assessing *Pth1r* gene expression in CFU-Ob cells from $Pth1r^{MALPs}$ mice, which was decreased by 90%. This cannot be reflected by the presence of only 4.08 ± 1.1% *tdTomato*+ bright cells, while the *tdTomato*+ dim cells represented 43.02 ± 1.74%, implying that *tdTomato*+ dim cells express *Adipoq* and are targeted by *AdipoqCre*. Zhou et al (Zhou et al., 2017) demonstrated that ~60% of CFU-F colonies formed by *AdipoqCreER;tdTomato*+ *Lepr*+ cells were Alizarin-Red-S+, implying that MALPs have the ability to undergo osteogenic differentiation *in vitro*. Therefore, while it is known that MALPs do not form bone-like structures *in vivo*, we showed that they exhibit cellular plasticity *in vitro*.

BMAT is considered functionally distinct from peripheral adipose tissues and accounts for greater than 10% of adipose tissue in the body (Liu et al., 2011, Mattiucci et al., 2018, Suchacki et al., 2020). Bone marrow adiposity gained interest with the growing evidence of its various functions, including adiponectin secretion, hematopoietic supporting factors secretion (SCF and CXCL12), driving tumor metastasis to bone, and most relevantly, RANKL production and regulation of skeletal homeostasis (Veldhuis-Vlug and Rosen, 2018, Morris and Edwards, 2019, Yu et al., 2020). A precursor to the

multi-functional bone marrow adipocyte is the MALP, which was recently described (Zhong et al., 2020). While lacking lipid droplets, MALPs are defined by their *Adipoq* expression, and are efficiently targeted by *AdipoqCre* (Zhong et al., 2020, Yu et al., 2020). While the *Adipoq*+ cells in the bone marrow were studied prior to the description of MALPs (Zhou et al., 2017), the role of MALPs in the context of skeletal homeostasis has not been fully elucidated. Zhong et al (Zhong et al., 2020) demonstrated an increase in trabecular bone mass following MALPs ablation, which was more pronounced in the diaphysis. Likewise, Zhou et al (Zou et al., 2020) showed an increase in trabecular and cortical bone mass with MALPs ablation. This was coupled with a brisk activation of osteoblastic differentiation. Both phenotypes were not reversed by fat transplantation, implying that MALPs suppress osteogenesis in a manner confined to the bone marrow environment. We show for the first time that PTH signaling in MALPs contributes to their regulation of skeletal homeostasis and that PTH exerts differential effects on different cell lineages, with opposite effects noted on the osteogenic and adipogenic lineages. We confirmed this phenotype *in vivo* and *in vitro*. First, an increase in trabecular bone mass was observed at 7 and 12 weeks of age, reflected by an increase in bone formation rate at 4 weeks of age in $Pth1r^{MALPs}$ mice. Second, while $Pth1r^{MALPs}$ mice had less progenitors *in vivo* and *in vitro*, they displayed comparable osteogenic differentiation potentials as the control mice, implying an enhanced osteogenic differentiation potential. Taken together, these data confirm that, contrary to its direct effect on BMSCs, PTH signaling in MALPs suppresses osteogenesis.

Increased bone marrow adipogenesis is part of several physiologic states such as puberty and aging, as well as pathologic alterations such as osteoporosis, diabetes,

and anorexia nervosa (Veldhuis-Vlug and Rosen, 2018). Intermittent PTH treatment decreases BMAT in osteoporotic men and women (Turner and Iwaniec, 2011, Yang et al., 2016, Fan et al., 2017). When $G_s\alpha$, a heterotrimeric G protein of the *Pth1r* (Cheloha et al., 2015), was deleted from *Osx*-expressing cells, the expansion in BMAT accompanied the decrease in trabecular bone (Sinha et al., 2014), confirming that PTH signaling suppresses adipogenesis. Additionally, by conditionally deleting *Pth1r* from *Prx1*-expressing bone marrow progenitors, Fan et al (Fan et al., 2017) demonstrated a dramatic decrease in trabecular and cortical bone mass, associated with an expansion of BMAT, concluding that PTH signaling in BMSC favors osteoblastic differentiation. *Prx1*-expressing cells are common progenitors to osteoblasts, chondrocytes, and adipocytes (Ambrosi et al., 2019). Given that bone marrow adipose lineage differentiates from a *Prx1*+ progenitor, we expected that PTH signaling in the adipose lineage suppresses adipogenesis in a manner parallel to that of the *Prx1*-expressing progenitor. Here, we delete the *Pth1r* only in the adipose lineage, which resulted in an increase in marrow adiposity, confirming that PTH signaling decreases adipogenesis.

RANKL is a key cytokine required for osteoclast differentiation and is known to be secreted from the osteoblast lineage (O'Brien, 2010, Xiong et al., 2015). Recently, Yu et al (Yu et al., 2020) reported a 15-fold increase in *Rankl* gene expression in MALPs compared to *Adipoq*- cells. We showed that MALPs exhibit a 14-fold increase in *Rankl* gene expression compared to *tdTomato*- cells. Additionally, the highest levels of ligand-receptor interaction with osteoclasts was observed in MALPs (Yu et al., 2020), confirming that MALPs are a major source of RANKL. It is long known that PTH increases RANKL production, particularly in the osteoblastic lineage (Fu et al., 2002,

Huang et al., 2004, Walker et al., 2012). However, it is not known whether PTH acts similarly on the adipogenic lineage. Upon *Pth1r* deletion in MSCs, Fan et al (Fan et al., 2017) demonstrated an increase in *Rankl* gene expression from BMAT. Consistently, we showed an increase in *Rankl* gene expression upon *Pth1r* deletion in the adipose lineage, coupled with an increase in osteoclast differentiation. Therefore, we conclude that PTH exhibits differential effects on *Rankl* expression depending on the cell lineage; while PTH induces *Rankl* expression in the osteoblast lineage, it suppresses *Rankl* expression in the adipose lineage.

Conclusions

Pth1r is expressed in many cell populations within the bone marrow, and the PTH signaling pathway plays a major role in the regulation of skeletal homeostasis (Lanske et al., 1996). Moreover, it is now evident that PTH signaling is involved not only in the regulation of bone mass but also in the regulation of BMAT. MALPs are a recently recognized cell population of adipogenic precursors within the bone marrow. The role of *Pth1r* in MALPs is not known. Our studies showed that PTH signaling in MALPs suppress osteogenesis by inhibiting the differentiation of progenitors. Furthermore, we confirmed that PTH signaling in the adipose lineage suppresses adipogenesis. Lastly, we showed that PTH signaling in MALPs suppress osteoclastogenesis, contrary to its effects on the osteoblast lineage.

Our current and ongoing experiments are focused on exploring the skeletal effects of intermittent PTH treatment in the absence of PTH signaling in MALPs and LiLA. Furthermore, we are describing the role of PTH on MALPs differentiation *ex vivo*.

Lastly, we are characterizing the genetic profiles of MALPs in the absence of PTH signaling.

Materials and methods

Generation of *AdipoqCre;Pth1r$^{fl/fl}$,TdTomato$^{fl/fl}$* conditional knockout mice

AdipoqCre;TdTomato$^{fl/fl}$ mice were purchased from Jackson Laboratory (Stock No. 028020). Floxed *Pth1r* mice were provided by B. Lanske. Floxed mice were crossed with *AdipoqCre;TdTomato$^{fl/fl}$* mice to obtain, *AdipoqCre;Pth1r$^{fl/fl}$,TdTomato$^{fl/fl}$* (*Pth1r^{MALPs}*). *AdipoqCre;TdTomato$^{fl/fl}$* mice and *Pth1r$^{fl/fl}$,TdTomato$^{fl/fl}$* were used as controls.

Animal studies

Animal studies were approved by the Harvard University Institutional Animal Care and Use Committee (IACUC). All mice were maintained in a pathogen-free, temperature- and light-controlled environment. Mice were identified by ear tags and genomic DNA (gDNA) was obtained from ear punches. Punched ear tissues were digested in 0.5 mL lysis buffer (1M Tris, 5M NaCl, 0.5M Ethylenediaminetetraacetic acid [EDTA] pH 8.0, 10% SDS) and proteinase K (20 mg/mL) at 55^{o} C and 850 rpm overnight. gDNA was isolated using 0.5 mL isopropyl alcohol and PCR-based genotyping was performed using GoTaq Green Master Mix (Promega Catalog #M7122).

Intraperitoneal injections were performed using two florescent labels to quantify bone formation rate. Four-week-old mice were injected with calcein (20 mg/kg) 3 days before bone collection and demeclocycline (40 mg/kg) + calcein (10 mg/kg) 1 day

before collection. Seven and twelve-week-old mice were injected with calcein 7 and 8 days before bone collection and demeclocycline + calcein 2 days before collection, respectively. Mice were euthanized at 4, 7 and 12 weeks of age using carbon dioxide inhalation followed by cervical dislocation. Cutaneous and visceral white adipose tissue was collected from inguinal (iWAT) and epididymal (eWAT) fat depots, respectively. Brown adipose tissue was collected from interscapular adipose tissue (iBAT). Tibiae, femurs and lumbar 3-5 vertebra were collected for skeletal phenotyping and gene expression assays.

Whole body images and organ images

Whole body images were obtained using Bruker MS FX Pro in-vivo animal imager and organ images were obtained using Leica MZ FL III Fluorescence Stereo Microscope.

μCT skeletal analysis

Tibiae were fixed in 70% ethanol and scanned using μCT35 (Scanco Medical AG, Brüttisellen, Switzerland). The bones were scanned at 55 kVP, 145 μA intensity, 200 msec integration time, 12 μm voxel size and 1000 projections/180^{o}. Cortical bone was measured in the mid-shaft region (75% the distance between the growth plate and the tibia-fibula junction) and extending 0.6 mm distally. The trabecular bone was measured 0.6 mm distal to the growth plate and extending 1.2 mm distally. A threshold of 394 mgHA/cm^3 was used for cortical bone and 303 mgHA/cm^3 was used for

trabecular bone. All μCT parameters were reported in accordance with previously published guidelines (Bouxsein et al., 2010).

Osmium staining and μCT BMAT analysis

Tibiae from 4- and 7-week-old mice were fixed in 10% neutral buffered formalin for at least 24 hours and processed as described previously (Scheller et al., 2014). Briefly, bones were washed under cold water for 1 hour and stored in PBS. Decalcification was carried out using 14% EDTA (pH 7.4) for 10-14 days depending on the mice age (changed every 3 days). Bones were washed 3 times using PBS (10 minutes each) and stained with 2% aqueous osmium tetroxide (Polysciences Catalog #23310-10) and 5% potassium dichromate for 48 hours. Bones were then washed and scanned at 55 kVP, 145 μA intensity, 300 msec integration time, 12 μm voxel size and 1000 projections/180^{o}. rBMAT was measured in the proximal one-third of the tibia, and cBMAT was measured in the distal one-third of the tibia. Parameters are reported according published guidelines (Bravenboer et al., 2019, Tratwal et al., 2020).

Histomorphometry

Tibiae were dissected from muscle, fixed in 70% ethanol for at least 24 hours, and dehydrated using acetone then embedded in methylmethacrylate (MMA). Undecalcified 4 μm-thick sections were obtained using a microtome and stained with Von Kossa stain to show the mineralized bone. A consecutive second section was left unstained for the analysis of fluorescence labeling, and a third section was stained with 2% Toluidine Blue (pH 3.7) to measure osteoid thickness and quantify osteoblasts. A

fourth section was stained with tartrate-resistant acid phosphatase (TRAP) to quantify osteoclasts. Only bi- and multinucleated cells were considered osteoclasts. Bone histomorphometric analysis was performed using OsteoMeasure analyzing software (Osteometrics Inc., Decatur, GA, USA) under X200 magnification. Trabecular bone was measured 0.45 um distal to the proximal growth plate and 0.9 mm in height and 1.3 mm in width. The structural parameters (bone volume [BV/TV], trabecular thickness [Tb.Th], trabecular number [Tb.N] and trabecular separation [Tb.Sp]) were obtained by calculating an average from the 3 consecutive sections. The structural, dynamic, and cellular parameters were reported according to the standardized nomenclature (Dempster et al., 2013).

Gene expression assays

RNA was extracted from freshly isolated or snap-frozen tissues and cells using RNeasy Plus Micro Kit (Qiagen Catalog #74034) or RNeasy Plus Mini Kit (Qiagen Catalog #74136) according to manufacturer's instructions. RNA was quantified using NanoDrop ND-1000 (Thermo Fisher Scientific) and cDNA was prepared using iScript™ cDNA Synthesis Kit (Bio-Rad catalog #1708891). Gene expression was determined using the conventional RT-qPCR method with Glyceraldehyde 3-phosphate dehydrogenase (Gapdh) and b2-microglobulin (B2M) as housekeeping genes. Fold change was reported as $2^{-\Delta\Delta CT}$.

Frozen sections and immunostaining

Tibiae were fixed using 4% paraformaldehyde at 4°C overnight, washed, and briefly decalcified using 10% EDTA solution for 3 days. After decalcifications, the bones were infiltrated with 30% sucrose overnight and embedded in optimal cutting temperature (OCT) compound. Ten µm-thick sections were obtained using Leica cryostat. After blocking, the frozen sections were incubated with Anti-Sp7 antibody (1:200; Abcam Catalog #ab209484) overnight at 4°C. After washing, the sections were then incubated with Alexa Fluor 488 goat anti-rabbit secondary antibody (1:200; Invitrogen Catalog #A-11008). Confocal images were obtained using Leica TCS SPE confocal microscope.

Serum biomarkers measurements

Blood was collected from the submandibular vein (at sacrifice) from 2-hour fasting mice. Sera were purified after centrifugation at 12500 rpm for 10 minutes and used for biochemical assays. Serum C-terminal telopeptide of type I collagen (CTX-I) levels were measured using RatLaps™ (CTX-I) EIA (Immunodiagnosticsystems Catalog #AC-06F1) and N-terminal propeptide of type I procollagen (PINP) levels were measured using Rat/Mouse PINP EIA (Immunodiagnosticsystems Catalog #AC-33F1) according to manufacturer's instructions.

Flow cytometry (FC) and florescence-assisted cell sorting (FACS)

Flushed bone marrow cells were resuspended in RBC Lysis Buffer (eBioscience Catalog # 00-4333-57) for 4 minutes. After adding 20 mL of PBS, cells were centrifuged at 500 x g for 5 minutes. PBS was decanted the cells were resuspended in 100 µL

FACS buffer (PBS with 2% FBS and 0.5 mM EDTA). Cells were incubated with 0.25 μg/10^6 cells TruStain FcX™ PLUS (BioLegend Catalog # 156604) for 15 minutes at 4° C in the dark to block non-specific IgG binding. Then, cells were incubated with the antibodies (**Flow cytometry and FACS antibodies table**). Cells were then washed twice using FACS buffer and incubated with 5-10 μl/test 7-Aminoactinomycin D (7-AAD, BioLegend Catalog #420403) for 10-15 minutes in the dark at 4° C immediately before FC/FACS. Alternatively, Live-or-Dye™ 750/777 Fixable Viability Staining Kit (Biotium Catalog # 32008) was used for dead cell exclusion. Flow cytometry was carried out using a four-laser Attune NxT Flow Cytometer (ThermoFisher Scientific) and FACS was carried out using BD™ LSR II. Compensation was performed using UltraComp eBeads Plus compensation beads (Thermo Fisher Scientific Catalog #01-3333-41) and florescence minus one (FMO) method. Cells were collected in culture medium when used for cell culture or RLT buffer for RNA extraction.

CFU assays

Bone marrow stromal cells were collected as described previously (Fan et al., 2017). Briefly, long bone ends were cut and bone marrow was flushed with ice-cold sterile phosphate buffered saline (PBS) using a needle and syringe. Cells were resuspended gently using a pipette and pelleted after centrifugation at 500 x g for 5 minutes. Supernatant was decanted and cells were gently resuspended in 1 mL of Red Blood Cell Lysing Buffer Hybri-Max (Sigma-Aldrich Catalog # R7757) for 30 seconds. After adding 12 mL of PBS, cells were centrifuged at 500 x g for 5 minutes. Supernatant was decanted and the cells were resuspended in α-MEM, 20% fetal bovine serum

(FBS) and 1% penicillin/streptomycin and plated at 3 x 10^6 cells/well in a 6-well plate. Cells were allowed to attach for 24 hours; non-adherent cells were aspirated, and media were changed subsequently according to the planned differentiation assay. For CFU-Ob, the culture medium was supplemented with 50 μg/ml ascorbic acid (Sigma Catalog #A5960) and 10 mM β-glycerophosphate (Sigma Catalog #G9422). For adipogenic differentiation, the culture medium was supplemented with 0.5 mM 3-Isobutyl-1-methylxanthine (IBMX; Sigma Catalog #I5879), 1 μM dexamethasone (Sigma Catalog #D4902), 10 μg/ml insulin (Sigma Catalog #I6634) and 1 μM rosiglitazone (Sigma Catalog #R2408) for the first two days. Then the adipogenic differentiation medium was switched to adipogenic base medium composed of 10 μg/ml insulin (Sigma Catalog #I6634) and 1 μM rosiglitazone (Sigma Catalog #R2408). A regular full medium was used for CFU-F for 10 days. For CFU-F, cells were stained with crystal violet after fixation with 10% formalin at day 10. For CFU-Ob and CFU-Ad, cells were stained with alkaline phosphatase (day 12) and oil red O (day 10) after fixation with 10% formalin, respectively. The percentage of stained area was measured using ImageJ software.

FACS sorted cells were collected in α-MEM culture medium supplemented with 20% fetal bovine serum (FBS), 1% penicillin/streptomycin, 20 mM L-Glutamine, and 0.1% 2-mercaptoethanol. Cells were collected in Eppendorfs and transferred to 0.1% gelatin-coated 12-well plates and seeded at 3000 cells/well (*tdTomato*+ bright and *tdTomato*+ dim), 10^5 cells/well for *tdTomato*-, and 10^6 cells/well for unfractionated whole bone marrow. Cells were incubated in a hypoxic incubator (10% CO_2 and 5% O_2). The culture medium was changed after 48 hours, and differentiation started at day 7.

Staining was carried out at day 10 of culture. Photomicrographs were obtained using Keyence BZ-X800 microscope.

Histology

Peripheral adipose tissues (iWAT, eWAT and iBAT) were fixed in 10% neutral buffered formalin for at least 24 hours and embedded in paraffin following fixation. Five µm-thick sections were obtained using a microtome and stained with hematoxylin and eosin. Photomicrographs were captured using cellSens imaging software (Olympus).

Statistics

Statistics were performed using Prism 8 (GraphPad San Diego, CA). All data were reported as mean ± standard error of the mean. Outliers were determined using ROUT method with Q = 1% and were excluded. Student's t-test was used to compare two groups and two-way ANOVA followed by Tukey's multiple comparisons was used for 3 or more groups. Alpha was set at 0.05. Illustrations are made using Biorender.com.

References

ADAMS, G. B., MARTIN, R. P., ALLEY, I. R., CHABNER, K. T., COHEN, K. S., CALVI, L. M., KRONENBERG, H. M. & SCADDEN, D. T. 2007. Therapeutic targeting of a stem cell niche. *Nat Biotechnol,* 25**,** 238-43.

AMBROSI, T. H., LONGAKER, M. T. & CHAN, C. K. F. 2019. A Revised Perspective of Skeletal Stem Cell Biology. *Front Cell Dev Biol,* 7**,** 189.

AMBROSI, T. H., SCIALDONE, A., GRAJA, A., GOHLKE, S., JANK, A. M., BOCIAN, C., WOELK, L., FAN, H., LOGAN, D. W., SCHURMANN, A., SARAIVA, L. R. & SCHULZ, T. J. 2017. Adipocyte Accumulation in the Bone Marrow during Obesity and Aging Impairs Stem Cell-Based Hematopoietic and Bone Regeneration. *Cell Stem Cell,* 20**,** 771-784 e6.

BACCIN, C., AL-SABAH, J., VELTEN, L., HELBLING, P. M., GRUNSCHLAGER, F., HERNANDEZ-MALMIERCA, P., NOMBELA-ARRIETA, C., STEINMETZ, L. M., TRUMPP, A. & HAAS, S. 2020. Combined single-cell and spatial transcriptomics reveal the molecular, cellular and spatial bone marrow niche organization. *Nat Cell Biol,* 22**,** 38-48.

BALANI, D. H., ONO, N. & KRONENBERG, H. M. 2017. Parathyroid hormone regulates fates of murine osteoblast precursors in vivo. *J Clin Invest,* 127**,** 3327-3338.

BARYAWNO, N., PRZYBYLSKI, D., KOWALCZYK, M. S., KFOURY, Y., SEVERE, N., GUSTAFSSON, K., KOKKALIARIS, K. D., MERCIER, F., TABAKA, M., HOFREE, M., DIONNE, D., PAPAZIAN, A., LEE, D., ASHENBERG, O., SUBRAMANIAN, A., VAISHNAV, E. D., ROZENBLATT-ROSEN, O., REGEV, A. & SCADDEN, D. T. 2019. A Cellular Taxonomy of the Bone Marrow Stroma in Homeostasis and Leukemia. *Cell,* 177**,** 1915-1932 e16.

BLACK, D. M. & ROSEN, C. J. 2016. Clinical Practice. Postmenopausal Osteoporosis. *N Engl J Med,* 374**,** 254-62.

BOUXSEIN, M. L., BOYD, S. K., CHRISTIANSEN, B. A., GULDBERG, R. E., JEPSEN, K. J. & MULLER, R. 2010. Guidelines for assessment of bone microstructure in rodents using micro-computed tomography. *J Bone Miner Res,* 25**,** 1468-86.

BRAVENBOER, N., BREDELLA, M. A., CHAUVEAU, C., CORSI, A., DOUNI, E., FERRIS, W. F., RIMINUCCI, M., ROBEY, P. G., ROJAS-SUTTERLIN, S., ROSEN, C., SCHULZ, T. J. & CAWTHORN, W. P. 2019. Standardised Nomenclature, Abbreviations, and Units for the Study of Bone Marrow Adiposity: Report of the Nomenclature Working Group of the International Bone Marrow Adiposity Society. *Front Endocrinol (Lausanne),* 10**,** 923.

CAIRE, R., ROCHE, B., PICOT, T., AANEI, C. M., HE, Z., CAMPOS, L., THOMAS, M., MALAVAL, L., VICO, L. & LAFAGE-PROUST, M. H. 2019. Parathyroid Hormone Remodels Bone Transitional Vessels and the Leptin Receptor-Positive Pericyte Network in Mice. *J Bone Miner Res,* 34**,** 1487-1501.

CALVI, L. M., ADAMS, G. B., WEIBRECHT, K. W., WEBER, J. M., OLSON, D. P., KNIGHT, M. C., MARTIN, R. P., SCHIPANI, E., DIVIETI, P., BRINGHURST, F. R., MILNER, L. A., KRONENBERG, H. M. & SCADDEN, D. T. 2003. Osteoblastic cells regulate the haematopoietic stem cell niche. *Nature,* 425**,** 841-6.

CALVI, L. M., SIMS, N. A., HUNZELMAN, J. L., KNIGHT, M. C., GIOVANNETTI, A., SAXTON, J. M., KRONENBERG, H. M., BARON, R. & SCHIPANI, E. 2001. Activated parathyroid hormone/parathyroid hormone-related protein receptor in osteoblastic cells differentially affects cortical and trabecular bone. *J Clin Invest,* 107**,** 277-86.

CHAN, C. K., SEO, E. Y., CHEN, J. Y., LO, D., MCARDLE, A., SINHA, R., TEVLIN, R., SEITA, J., VINCENT-TOMPKINS, J., WEARDA, T., LU, W. J., SENARATH-YAPA, K., CHUNG, M. T., MARECIC, O., TRAN, M., YAN, K. S., UPTON, R., WALMSLEY, G. G., LEE, A. S., SAHOO, D., KUO, C. J., WEISSMAN, I. L. & LONGAKER, M. T. 2015. Identification and specification of the mouse skeletal stem cell. *Cell,* 160**,** 285-98.

CHELOHA, R. W., GELLMAN, S. H., VILARDAGA, J. P. & GARDELLA, T. J. 2015. PTH receptor-1 signalling-mechanistic insights and therapeutic prospects. *Nat Rev Endocrinol,* 11**,** 712-24.

DELGADO-CALLE, J., TU, X., PACHECO-COSTA, R., MCANDREWS, K., EDWARDS, R., PELLEGRINI, G. G., KUHLENSCHMIDT, K., OLIVOS, N., ROBLING, A., PEACOCK, M., PLOTKIN, L. I. & BELLIDO, T. 2017. Control of Bone Anabolism in Response to Mechanical Loading and

PTH by Distinct Mechanisms Downstream of the PTH Receptor. *J Bone Miner Res,* 32**,** 522-535.

DEMPSTER, D. W., COMPSTON, J. E., DREZNER, M. K., GLORIEUX, F. H., KANIS, J. A., MALLUCHE, H., MEUNIER, P. J., OTT, S. M., RECKER, R. R. & PARFITT, A. M. 2013. Standardized nomenclature, symbols, and units for bone histomorphometry: a 2012 update of the report of the ASBMR Histomorphometry Nomenclature Committee. *J Bone Miner Res,* 28**,** 2-17.

DING, L. & MORRISON, S. J. 2013. Haematopoietic stem cells and early lymphoid progenitors occupy distinct bone marrow niches. *Nature,* 495**,** 231-5.

DING, L., SAUNDERS, T. L., ENIKOLOPOV, G. & MORRISON, S. J. 2012. Endothelial and perivascular cells maintain haematopoietic stem cells. *Nature,* 481**,** 457-62.

FAIRFIELD, H., FALANK, C., AVERY, L. & REAGAN, M. R. 2016. Multiple myeloma in the marrow: pathogenesis and treatments. *Ann N Y Acad Sci,* 1364**,** 32-51.

FAN, Y., HANAI, J. I., LE, P. T., BI, R., MARIDAS, D., DEMAMBRO, V., FIGUEROA, C. A., KIR, S., ZHOU, X., MANNSTADT, M., BARON, R., BRONSON, R. T., HOROWITZ, M. C., WU, J. Y., BILEZIKIAN, J. P., DEMPSTER, D. W., ROSEN, C. J. & LANSKE, B. 2017. Parathyroid Hormone Directs Bone Marrow Mesenchymal Cell Fate. *Cell Metab,* 25**,** 661-672.

FU, Q., JILKA, R. L., MANOLAGAS, S. C. & O'BRIEN, C. A. 2002. Parathyroid hormone stimulates receptor activator of NFkappa B ligand and inhibits osteoprotegerin expression via protein kinase A activation of cAMP-response element-binding protein. *J Biol Chem,* 277**,** 48868-75.

GARDINIER, J. D., DALY-SEILER, C., ROSTAMI, N., KUNDAL, S. & ZHANG, C. 2019. Loss of the PTH/PTHrP receptor along the osteoblast lineage limits the anabolic response to exercise. *PLoS One,* 14**,** e0211076.

HEFFNER, C. S., HERBERT PRATT, C., BABIUK, R. P., SHARMA, Y., ROCKWOOD, S. F., DONAHUE, L. R., EPPIG, J. T. & MURRAY, S. A. 2012. Supporting conditional mouse mutagenesis with a comprehensive cre characterization resource. *Nat Commun,* 3**,** 1218.

HUANG, J. C., SAKATA, T., PFLEGER, L. L., BENCSIK, M., HALLORAN, B. P., BIKLE, D. D. & NISSENSON, R. A. 2004. PTH differentially regulates expression of RANKL and OPG. *J Bone Miner Res,* 19**,** 235-44.

JOHNSTON, C. B. & DAGAR, M. 2020. Osteoporosis in Older Adults. *Med Clin North Am,* 104**,** 873-884.

KANIS, J. A., COOPER, C., RIZZOLI, R., REGINSTER, J. Y., SCIENTIFIC ADVISORY BOARD OF THE EUROPEAN SOCIETY FOR, C., ECONOMIC ASPECTS OF, O., THE COMMITTEES OF SCIENTIFIC, A. & NATIONAL SOCIETIES OF THE INTERNATIONAL OSTEOPOROSIS, F. 2019. European guidance for the diagnosis and management of osteoporosis in postmenopausal women. *Osteoporos Int,* 30**,** 3-44.

KIR, S., KOMABA, H., GARCIA, A. P., ECONOMOPOULOS, K. P., LIU, W., LANSKE, B., HODIN, R. A. & SPIEGELMAN, B. M. 2016. PTH/PTHrP Receptor Mediates Cachexia in Models of Kidney Failure and Cancer. *Cell Metab,* 23**,** 315-23.

KURENKOVA, A. D., MEDVEDEVA, E. V., NEWTON, P. T. & CHAGIN, A. S. 2020. Niches for Skeletal Stem Cells of Mesenchymal Origin. *Front Cell Dev Biol,* 8**,** 592.

KUSUMBE, A. P., RAMASAMY, S. K. & ADAMS, R. H. 2014. Coupling of angiogenesis and osteogenesis by a specific vessel subtype in bone. *Nature,* 507**,** 323-328.

LANSKE, B., KARAPLIS, A. C., LEE, K., LUZ, A., VORTKAMP, A., PIRRO, A., KARPERIEN, M., DEFIZE, L. H., HO, C., MULLIGAN, R. C., ABOU-SAMRA, A. B., JÜPPNER, H., SEGRE, G. V. & KRONENBERG, H. M. 1996. PTH/PTHrP receptor in early development and Indian hedgehog-regulated bone growth. *Science,* 273**,** 663-6.

LI, C., XING, Q., YU, B., XIE, H., WANG, W., SHI, C., CRANE, J. L., CAO, X. & WAN, M. 2013. Disruption of LRP6 in osteoblasts blunts the bone anabolic activity of PTH. *J Bone Miner Res,* 28**,** 2094-108.

LIU, L. F., SHEN, W. J., UENO, M., PATEL, S. & KRAEMER, F. B. 2011. Characterization of age-related gene expression profiling in bone marrow and epididymal adipocytes. *BMC Genomics,* 12**,** 212.

MATSUSHITA, Y., NAGATA, M., KOZLOFF, K. M., WELCH, J. D., MIZUHASHI, K., TOKAVANICH, N., HALLETT, S. A., LINK, D. C., NAGASAWA, T., ONO, W. & ONO, N. 2020. A Wnt-mediated transformation of the bone marrow stromal cell identity orchestrates skeletal regeneration. *Nat Commun,* 11**,** 332.

MATTIUCCI, D., MAURIZI, G., IZZI, V., CENCI, L., CIARLANTINI, M., MANCINI, S., MENSA, E., PASCARELLA, R., VIVARELLI, M., OLIVIERI, A., LEONI, P. & POLONI, A. 2018. Bone marrow adipocytes support hematopoietic stem cell survival. *J Cell Physiol,* 233**,** 1500-1511.

MCDONALD, M. M., FAIRFIELD, H., FALANK, C. & REAGAN, M. R. 2017. Adipose, Bone, and Myeloma: Contributions from the Microenvironment. *Calcif Tissue Int,* 100**,** 433-448.

MORIKAWA, S., MABUCHI, Y., KUBOTA, Y., NAGAI, Y., NIIBE, K., HIRATSU, E., SUZUKI, S., MIYAUCHI-HARA, C., NAGOSHI, N., SUNABORI, T., SHIMMURA, S., MIYAWAKI, A., NAKAGAWA, T., SUDA, T., OKANO, H. & MATSUZAKI, Y. 2009. Prospective identification, isolation, and systemic transplantation of multipotent mesenchymal stem cells in murine bone marrow. *J Exp Med,* 206**,** 2483-96.

MORRIS, E. V. & EDWARDS, C. M. 2019. Bone marrow adiposity and multiple myeloma. *Bone,* 118**,** 42-46.

NEER, R. M., ARNAUD, C. D., ZANCHETTA, J. R., PRINCE, R., GAICH, G. A., REGINSTER, J. Y., HODSMAN, A. B., ERIKSEN, E. F., ISH-SHALOM, S., GENANT, H. K., WANG, O. & MITLAK, B. H. 2001. Effect of parathyroid hormone (1-34) on fractures and bone mineral density in postmenopausal women with osteoporosis. *N Engl J Med,* 344**,** 1434-41.

O'BRIEN, C. A. 2010. Control of RANKL gene expression. *Bone,* 46**,** 911-9.

OGURO, H., DING, L. & MORRISON, S. J. 2013. SLAM family markers resolve functionally distinct subpopulations of hematopoietic stem cells and multipotent progenitors. *Cell Stem Cell,* 13**,** 102-16.

OMATSU, Y., SUGIYAMA, T., KOHARA, H., KONDOH, G., FUJII, N., KOHNO, K. & NAGASAWA, T. 2010. The essential functions of adipo-osteogenic progenitors as the hematopoietic stem and progenitor cell niche. *Immunity,* 33**,** 387-99.

QIU, T., XIAN, L., CRANE, J., WEN, C., HILTON, M., LU, W., NEWMAN, P. & CAO, X. 2015. PTH receptor signaling in osteoblasts regulates endochondral vascularization in maintenance of postnatal growth plate. *J Bone Miner Res,* 30**,** 309-17.

SCHELLER, E. L., TROIANO, N., VANHOUTAN, J. N., BOUXSEIN, M. A., FRETZ, J. A., XI, Y., NELSON, T., KATZ, G., BERRY, R., CHURCH, C. D., DOUCETTE, C. R., RODEHEFFER, M. S., MACDOUGALD, O. A., ROSEN, C. J. & HOROWITZ, M. C. 2014. Use of osmium tetroxide

staining with microcomputerized tomography to visualize and quantify bone marrow adipose tissue in vivo. *Methods Enzymol,* 537**,** 123-39.

SINHA, P., AARNISALO, P., CHUBB, R., ONO, N., FULZELE, K., SELIG, M., SAEED, H., CHEN, M., WEINSTEIN, L. S., PAJEVIC, P. D., KRONENBERG, H. M. & WU, J. Y. 2014. Loss of Gsalpha early in the osteoblast lineage favors adipogenic differentiation of mesenchymal progenitors and committed osteoblast precursors. *J Bone Miner Res,* 29**,** 2414-26.

SUCHACKI, K. J., TAVARES, A. A. S., MATTIUCCI, D., SCHELLER, E. L., PAPANASTASIOU, G., GRAY, C., SINTON, M. C., RAMAGE, L. E., MCDOUGALD, W. A., LOVDEL, A., SULSTON, R. J., THOMAS, B. J., NICHOLSON, B. M., DRAKE, A. J., ALCAIDE-CORRAL, C. J., SAID, D., POLONI, A., CINTI, S., MACPHERSON, G. J., DWECK, M. R., ANDREWS, J. P. M., WILLIAMS, M. C., WALLACE, R. J., VAN BEEK, E. J. R., MACDOUGALD, O. A., MORTON, N. M., STIMSON, R. H. & CAWTHORN, W. P. 2020. Bone marrow adipose tissue is a unique adipose subtype with distinct roles in glucose homeostasis. *Nat Commun,* 11**,** 3097.

TIKHONOVA, A. N., DOLGALEV, I., HU, H., SIVARAJ, K. K., HOXHA, E., CUESTA-DOMINGUEZ, A., PINHO, S., AKHMETZYANOVA, I., GAO, J., WITKOWSKI, M., GUILLAMOT, M., GUTKIN, M. C., ZHANG, Y., MARIER, C., DIEFENBACH, C., KOUSTENI, S., HEGUY, A., ZHONG, H., FOOKSMAN, D. R., BUTLER, J. M., ECONOMIDES, A., FRENETTE, P. S., ADAMS, R. H., SATIJA, R., TSIRIGOS, A. & AIFANTIS, I. 2019. The bone marrow microenvironment at single-cell resolution. *Nature,* 569**,** 222-228.

TRATWAL, J., LABELLA, R., BRAVENBOER, N., KERCKHOFS, G., DOUNI, E., SCHELLER, E. L., BADR, S., KARAMPINOS, D. C., BECK-CORMIER, S., PALMISANO, B., POLONI, A., MORENO-ALIAGA, M. J., FRETZ, J., RODEHEFFER, M. S., BOROUMAND, P., ROSEN, C. J., HOROWITZ, M. C., VAN DER EERDEN, B. C. J., VELDHUIS-VLUG, A. G. & NAVEIRAS, O. 2020. Reporting Guidelines, Review of Methodological Standards, and Challenges Toward Harmonization in Bone Marrow Adiposity Research. Report of the Methodologies Working Group of the International Bone Marrow Adiposity Society. *Front Endocrinol (Lausanne),* 11**,** 65.

TURNER, R. T. & IWANIEC, U. T. 2011. Low dose parathyroid hormone maintains normal bone formation in adult male rats during rapid weight loss. *Bone,* 48**,** 726-32.

VELDHUIS-VLUG, A. G. & ROSEN, C. J. 2018. Clinical implications of bone marrow adiposity. *J Intern Med,* 283**,** 121-139.

WALKER, E. C., POULTON, I. J., MCGREGOR, N. E., HO, P. W., ALLAN, E. H., QUACH, J. M., MARTIN, T. J. & SIMS, N. A. 2012. Sustained RANKL response to parathyroid hormone in oncostatin M receptor-deficient osteoblasts converts anabolic treatment to a catabolic effect in vivo. *J Bone Miner Res,* 27**,** 902-12.

WEIN, M. N. & KRONENBERG, H. M. 2018. Regulation of Bone Remodeling by Parathyroid Hormone. *Cold Spring Harb Perspect Med,* 8.

WOLOCK, S. L., KRISHNAN, I., TENEN, D. E., MATKINS, V., CAMACHO, V., PATEL, S., AGARWAL, P., BHATIA, R., TENEN, D. G., KLEIN, A. M. & WELNER, R. S. 2019. Mapping Distinct Bone Marrow Niche Populations and Their Differentiation Paths. *Cell Rep,* 28**,** 302-311 e5.

WORTHLEY, D. L., CHURCHILL, M., COMPTON, J. T., TAILOR, Y., RAO, M., SI, Y., LEVIN, D., SCHWARTZ, M. G., UYGUR, A., HAYAKAWA, Y., GROSS, S., RENZ, B. W., SETLIK, W., MARTINEZ, A. N., CHEN, X., NIZAMI, S., LEE, H. G., KANG, H. P., CALDWELL, J. M., ASFAHA, S., WESTPHALEN, C. B., GRAHAM, T., JIN, G., NAGAR, K., WANG, H., KHEIRBEK, M. A., KOLHE, A., CARPENTER, J., GLAIRE, M., NAIR, A., RENDERS, S., MANIERI, N.,

MUTHUPALANI, S., FOX, J. G., REICHERT, M., GIRAUD, A. S., SCHWABE, R. F., PRADERE, J. P., WALTON, K., PRAKASH, A., GUMUCIO, D., RUSTGI, A. K., STAPPENBECK, T. S., FRIEDMAN, R. A., GERSHON, M. D., SIMS, P., GRIKSCHEIT, T., LEE, F. Y., KARSENTY, G., MUKHERJEE, S. & WANG, T. C. 2015. Gremlin 1 identifies a skeletal stem cell with bone, cartilage, and reticular stromal potential. *Cell,* 160**,** 269-84.

XIONG, J., PIEMONTESE, M., ONAL, M., CAMPBELL, J., GOELLNER, J. J., DUSEVICH, V., BONEWALD, L., MANOLAGAS, S. C. & O'BRIEN, C. A. 2015. Osteocytes, not Osteoblasts or Lining Cells, are the Main Source of the RANKL Required for Osteoclast Formation in Remodeling Bone. *PLoS One,* 10**,** e0138189.

XIONG, J., PIEMONTESE, M., THOSTENSON, J. D., WEINSTEIN, R. S., MANOLAGAS, S. C. & O'BRIEN, C. A. 2014. Osteocyte-derived RANKL is a critical mediator of the increased bone resorption caused by dietary calcium deficiency. *Bone,* 66**,** 146-54.

YANG, Y., LUO, X., XIE, X., YAN, F., CHEN, G., ZHAO, W., JIANG, Z., FANG, C. & SHEN, J. 2016. Influences of teriparatide administration on marrow fat content in postmenopausal osteopenic women using MR spectroscopy. *Climacteric,* 19**,** 285-91.

YU, B., ZHAO, X., YANG, C., CRANE, J., XIAN, L., LU, W., WAN, M. & CAO, X. 2012. Parathyroid hormone induces differentiation of mesenchymal stromal/stem cells by enhancing bone morphogenetic protein signaling. *J Bone Miner Res,* 27**,** 2001-14.

YU, W., ZHONG, L., YAO, L., WEI, Y., GUI, T., LI, Z., KIM, H., HOLDREITH, N., JIANG, X., TONG, W., DYMENT, N. A., LIU, X. S., YANG, S., CHOI, Y., AHN, J. & QIN, L. 2020. Bone marrow adipogenic lineage precursors (MALPs) promote osteoclastogenesis in bone remodeling and pathologic bone loss. *J Clin Invest*.

ZHONG, L., YAO, L., TOWER, R. J., WEI, Y., MIAO, Z., PARK, J., SHRESTHA, R., WANG, L., YU, W., HOLDREITH, N., HUANG, X., ZHANG, Y., TONG, W., GONG, Y., AHN, J., SUSZTAK, K., DYMENT, N., LI, M., LONG, F., CHEN, C., SEALE, P. & QIN, L. 2020. Single cell transcriptomics identifies a unique adipose lineage cell population that regulates bone marrow environment. *Elife,* 9.

ZHOU, B. O., YU, H., YUE, R., ZHAO, Z., RIOS, J. J., NAVEIRAS, O. & MORRISON, S. J. 2017. Bone marrow adipocytes promote the regeneration of stem cells and haematopoiesis by secreting SCF. *Nat Cell Biol,* 19**,** 891-903.

ZOU, W., ROHATGI, N., BRESTOFF, J. R., LI, Y., BARVE, R. A., TYCKSEN, E., KIM, Y., SILVA, M. J. & TEITELBAUM, S. L. 2020. Ablation of Fat Cells in Adult Mice Induces Massive Bone Gain. *Cell Metab*.

Figures:

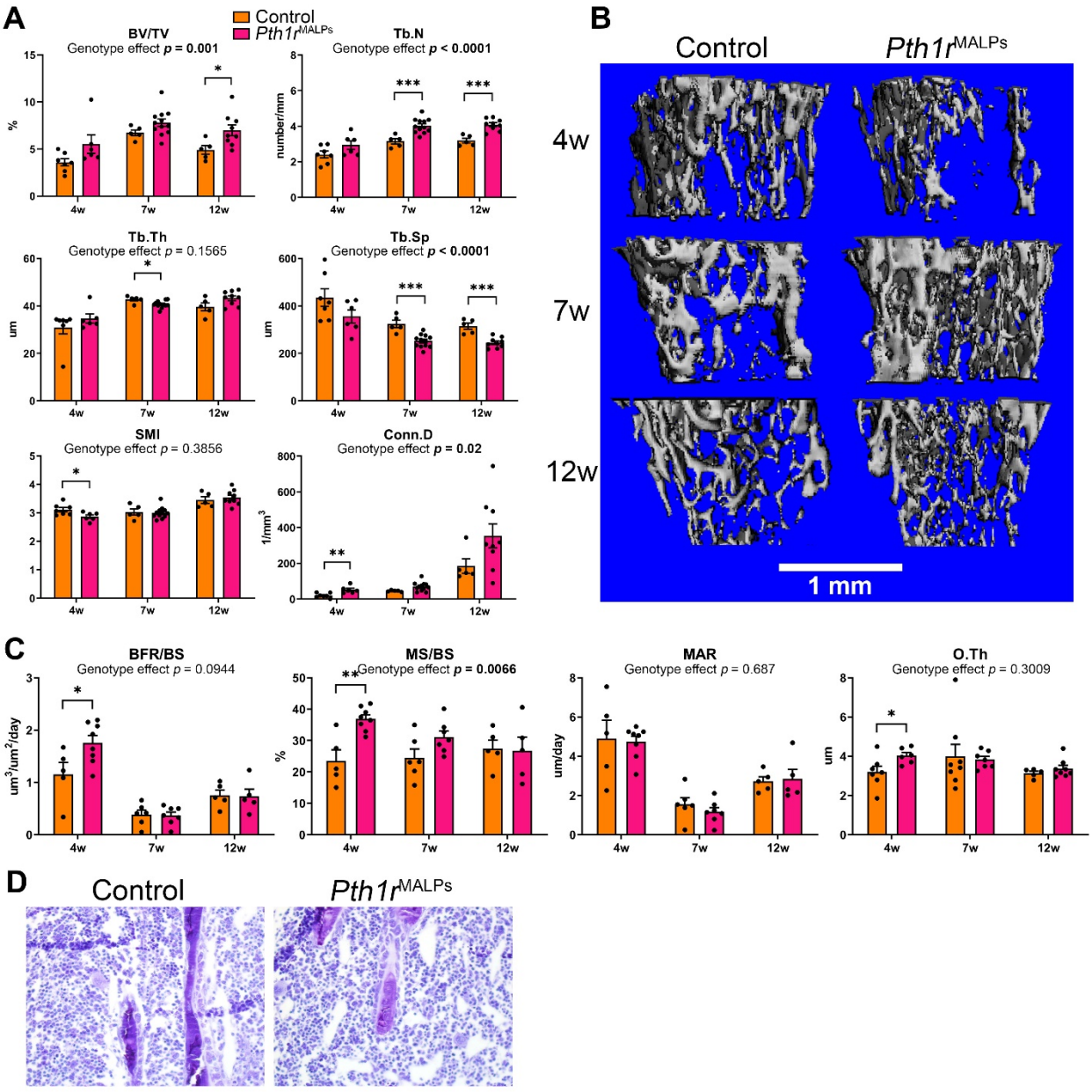

Figure 1: PTH signaling in MALPs suppresses osteogenesis.

A) µCT analysis of trabecular bone in the proximal tibia of *Pth1r*^{MALPs} female mice and littermate controls. *Pth1r*^{MALPs} mice had an increase in bone volume at 12 weeks of age, coupled with an increase in trabecular number and trabecular thickness (n=5-12;

genotype effect calculated by two-way ANOVA; * $p < 0.05$, ** $p < 0.01$, *** $p < 0.001$, **** $p < 0.0001$ by Student's t-test).

B) Representative images of 3-dimentional (3-D) reconstruction of trabecular bone. Note the increase in bone volume particularly at 12 weeks of age.

C) Dynamic histomorphometry analysis of proximal tibia. *Pth1r*^{MALPs} mice exhibited an increase in bone formation rate, mineralized surface, and osteoid thickness (n=5-8; genotype effect calculated by two-way ANOVA; * $p < 0.05$, ** $p < 0.01$, *** $p < 0.001$, **** $p < 0.0001$ by Student's t-test).

D) Representative photomicrographs of toluidine blue staining. *Pth1r*^{MALPs} mice exhibited an increase in osteoid thickness (original magnification X400).

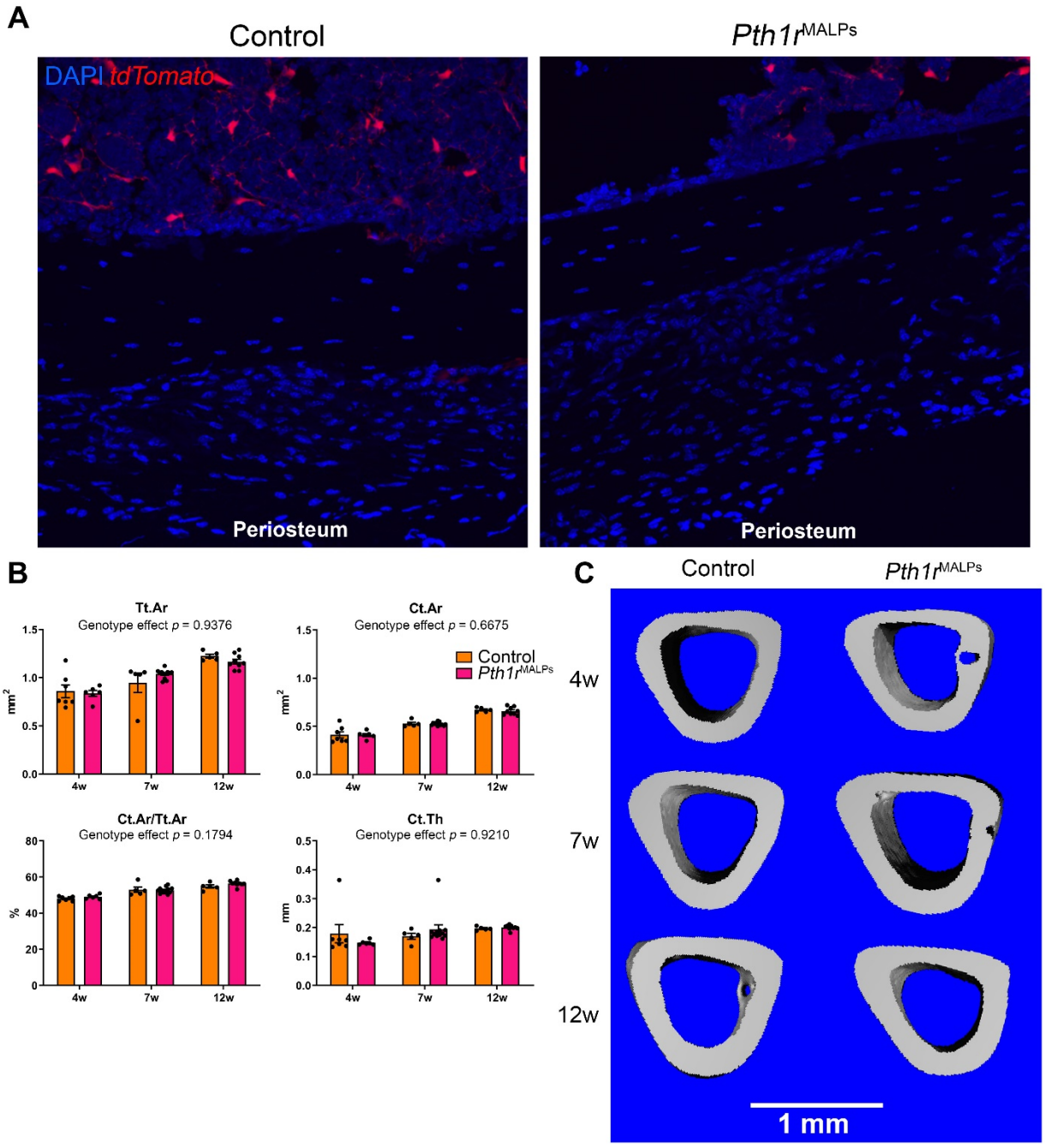

Figure 2: Loss of PTH signaling in MALPs does not affect the cortical bone.

A) Representative photomicrographs of *tdTomato* florescent labelling. *tdTomato*+ cells are non-existent on the periosteal surface.

B) µCT analysis of cortical bone in mid-shaft tibia of *Pth1r*^{MALPs} female mice and littermate controls. *Pth1r*^{MALPs} mice and littermate controls have similar cortical bone volume and thickness (n=5-12; genotype effect calculated by two-way ANOVA).
C) Representative images of 3-D reconstruction of cortical bone.

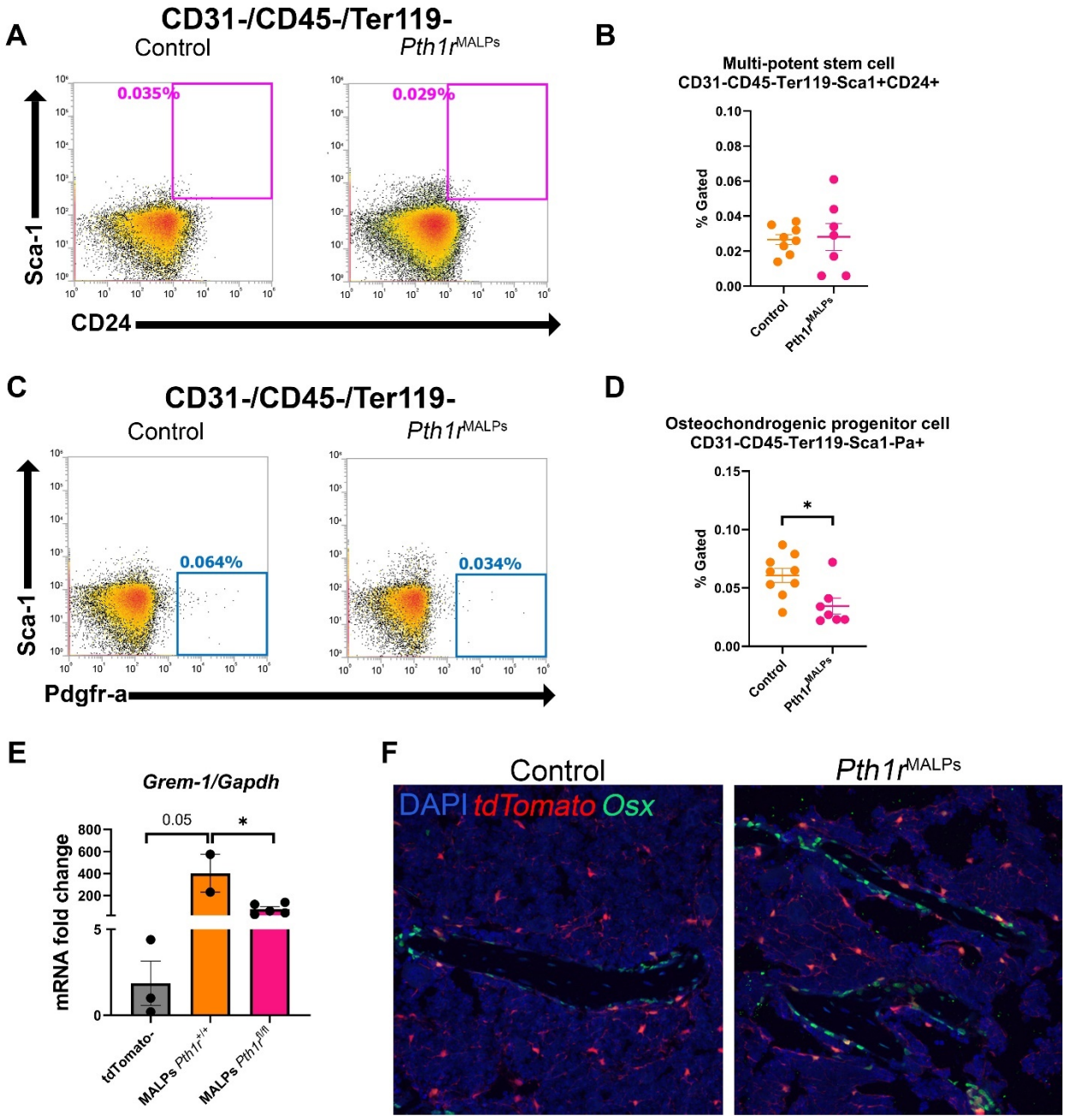

Figure 3: PTH signaling in MALPs maintains osteochondroprogenitors by suppressing their differentiation into mature osteoblasts.

A) Representative flow cytometry density plots of MSC population from flushed bone marrow from 4-week-old *Pth1r*^{MALPs} mice and littermate controls. Live cells were gated based on CD31-/CD45-/Ter119-.

B) Quantification of MSCs. *Pth1r*^{MALPs} mice had a similar MSC proportion as the littermate controls.

C) Representative flow cytometry density plots of OPC population from flushed bone marrow from 4-week-old *Pth1r*^{MALPs} mice and littermate controls. Live cells were gated based on CD31-/CD45-/Ter119-.

D) Quantification of OPCs. *Pth1r*^{MALPs} mice exhibited a decrease in OPC percentage by half (n=7-8/group, Student's t-test, * $p < 0.05$).

E) *Grem1* gene expression is increased in MALPs by ~400 fold compared to *tdTomato*- cells. MALPs from *Pth1r*^{MALPs} mice exhibit an 80% decrease in *Grem1* expression (n=5-5/group, Student's t-test, * $p < 0.05$).

F) Representative florescent photomicrographs of *tdTomato*+ and *Osx*+ cells. *Pth1r*^{MALPs} mice exhibit a mild increase in *Osx*+ cells.

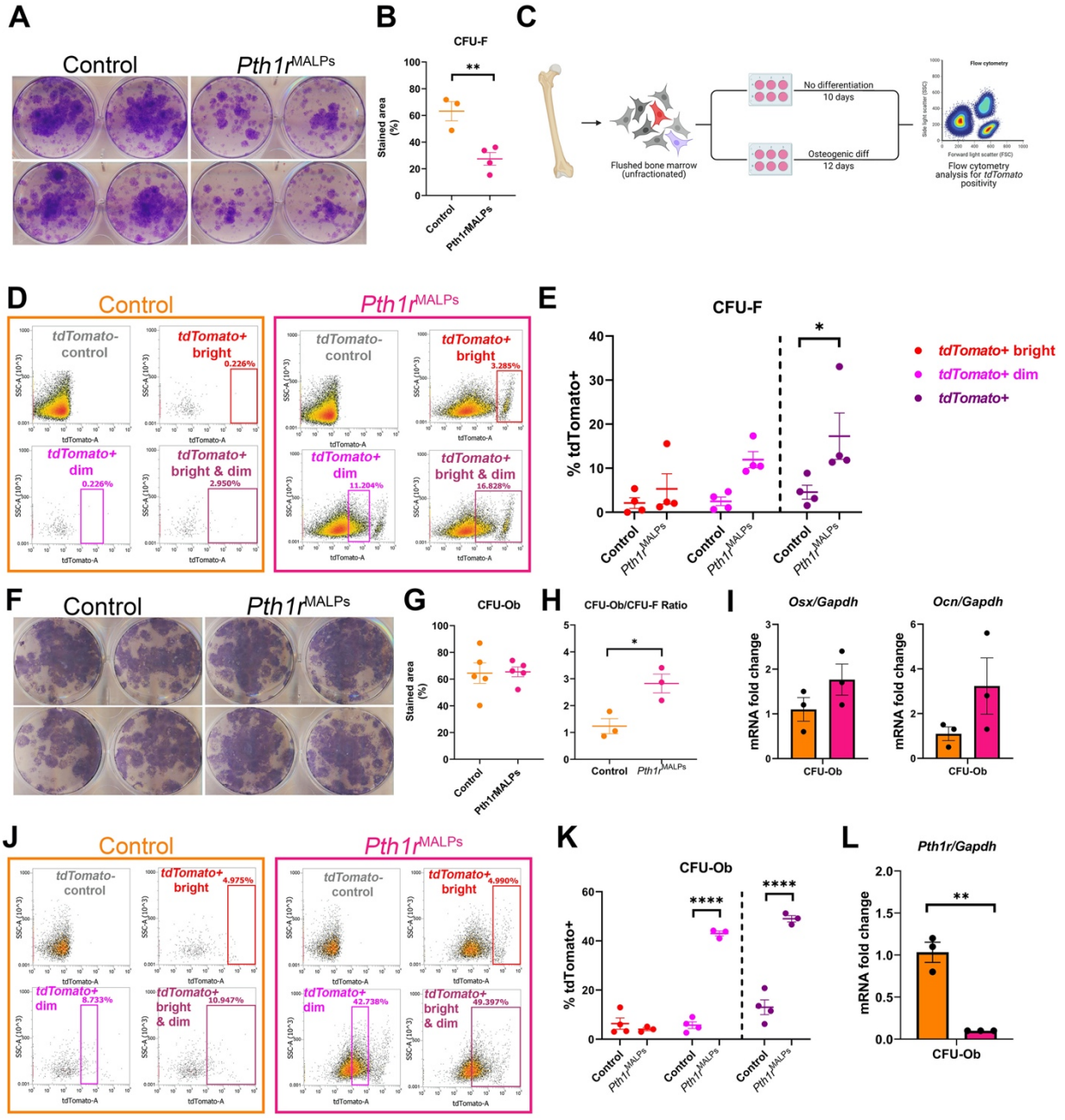

Figure 4: Loss of PTH signaling in MALPs decreases bone marrow progenitors by increasing their differentiation into osteoblasts.

A) Crystal violet staining of CFU-F cells showed a notable decrease in bone marrow progenitors in *Pth1r*^{MALPs} mice.

B) Quantification of the stained area. Cells from *Pth1r*^{MALPs} mice exhibited a significant decrease in CFU-F (n=3-4 experiments/group, each experiment was performed in duplicate, Student's t-test, * $p < 0.05$).

C) Experimental design of cultured unfractionated flushed bone marrow cells. *tdTomato* positivity was assessed after 10 days of culture for CFU-F and 12 days of culture for CFU-Ob.

D) Representative flow cytometry density plots of *tdTomato*- control, *tdTomato*+ dim, *tdTomato*+ bright, and overall *tdTomato*+.

E) Quantification of *tdTomato*+ dim, *tdTomato*+ bright, and overall *tdTomato*+ cells in CFU-F. Less than 10% of CFU-F cells were *tdTomato*+ in the control group. Cells from *Pth1r*^{MALPs} mice exhibited an increase in *tdTomato*+ dim cells (n=3-4 experiments/group, each experiment was performed in duplicate, Student's t-test, * $p < 0.05$).

F) Alkaline phosphatase staining of CFU-Ob cells showed comparable osteogenic differentiation potentials between *Pth1r*^{MALPs} mice and littermate controls.

G) Quantification of the stained area (n=5 experiments, each experiment was performed in duplicate).

H) CFU-Ob/CFU-F ratio was significantly increased in cells from *Pth1r*^{MALPs} mice (n=3 experiments/group, each experiment was performed in duplicate, Student's t-test, * $p < 0.05$).

I) RT-qPCR analysis of *Osx* and *osteocalcin* (*Ocn*) gene expression from CFU-Ob cells revealed a slight increase in osteoblast differentiation genes (n=3 experiments/group, each experiment was performed in duplicate).

J) Representative flow cytometry density plots of *tdTomato*+ bright, *tdTomato*+ dim, and combined *tdTomato*+ cells from CFU-Ob cells.

K) Quantification of *tdTomato* positivity stratified by *tdTomato* signal intensity (n=3 experiments, each experiment was performed in duplicate).

L) RT-qPCR analysis of unfractionated CFU-Ob cells revealed a 90.3% decrease in *Pth1r* mRNA gene expression (n=3 experiments/group, each experiment was performed in duplicate, Student's t-test, ** $p < 0.01$).

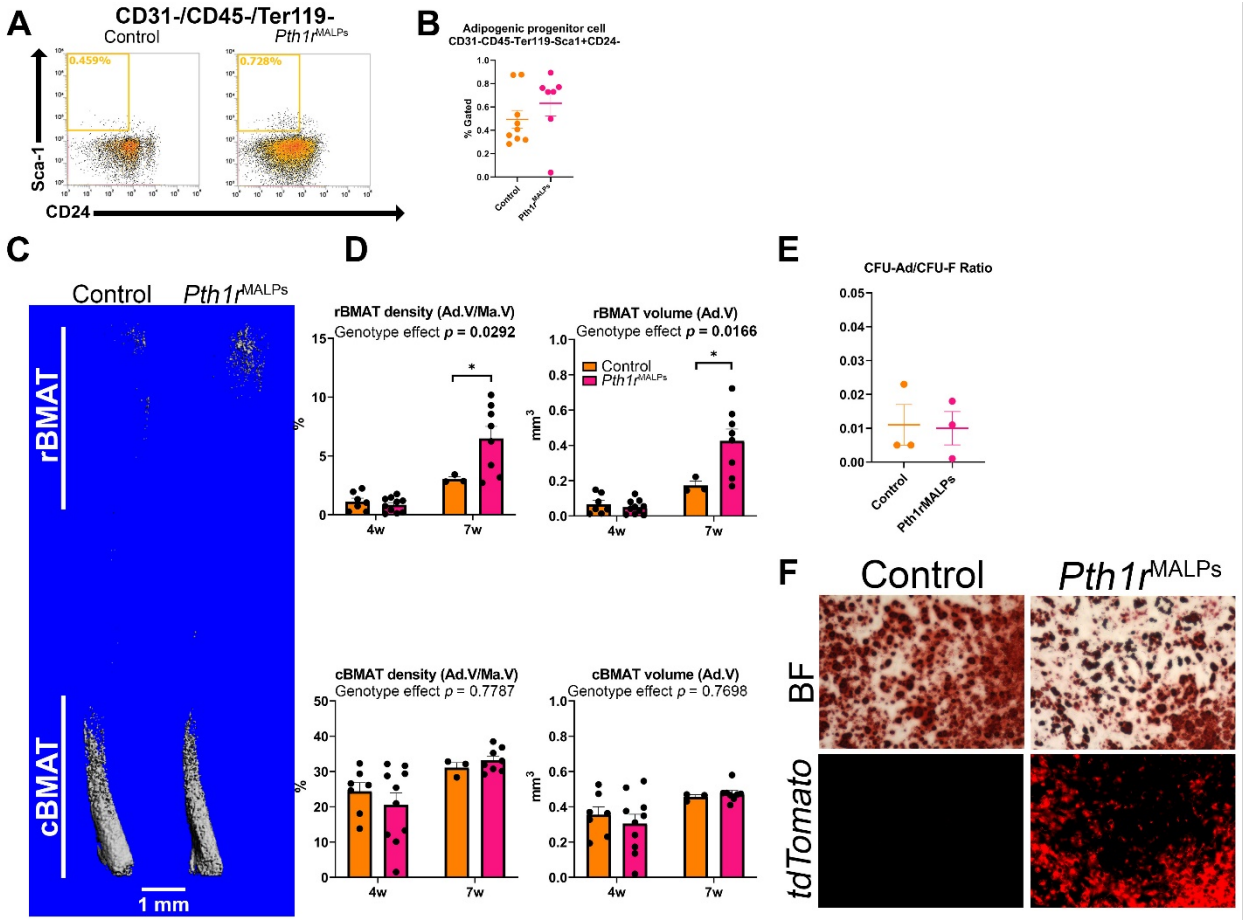

Figure 5: PTH signaling in MALPs suppresses adipogenesis.

A) Representative flow cytometry density plots of APC population from flushed bone marrow cells. Live cells were gated based on CD31-/CD45-/Ter119-.

B) Quantification of APCs from *Pth1r*^{MALPs} mice and littermate controls showed a 28% non-significant increase in APC percentage in *Pth1r*^{MALPs} mice (n=7-9/group).

C) Representative 3-D reconstruction of osmium-stained tibiae of 7-week-old female mice.

D) Quantification of BMAT volume and density in rBMAT and cBMAT. Seven-week-old *Pth1r*^{MALPs} mice had a higher rBMAT volume and density (n=3-10; genotype effect calculated by two-way ANOVA; * $p < 0.05$, ** $p < 0.01$, *** $p < 0.001$, **** $p < 0.0001$ by Student's t-test).

E) *Pth1r*^{MALPs} mice and littermate controls had a similar CFU-Ad/CFU-F ratio.

F) Photomicrographs of CFU-Ad colonies. The majority of cells within the CFU-Ad colonies were *tdTomato*+ (original magnification X200).

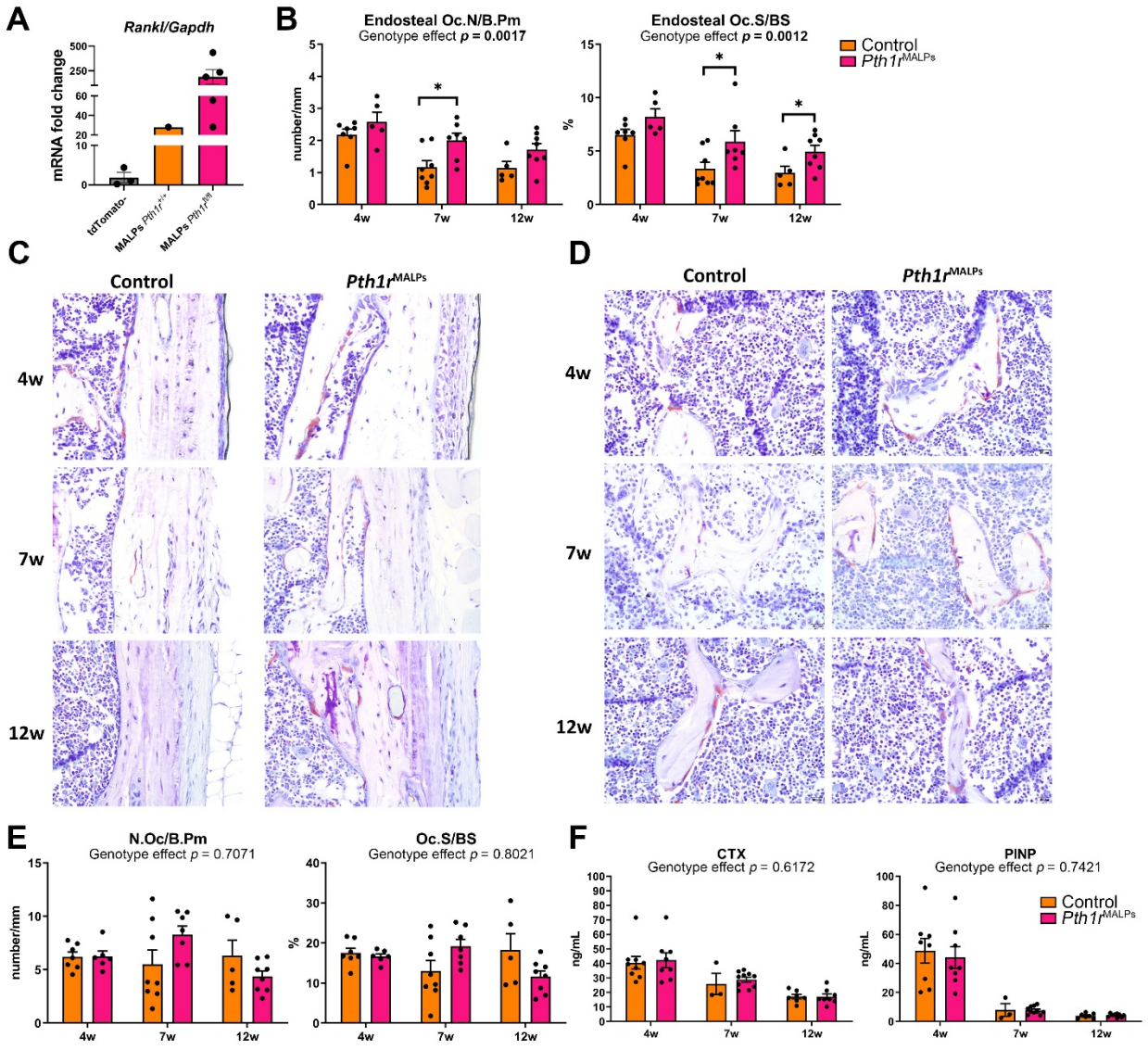

Figure 6: PTH signaling in MALPs suppresses osteoclastogenesis.

A) MALPs exhibit a ~14-fold increase in *Rankl* gene expression compared to *tdTomato-* cells and deletion of Pth1r in MALPs increases Rankl expression by ~7 folds (n=1-5/group).

B) Quantitative analysis of TRAP+ cells on the endosteal surface revealed an increase in osteoclast number and surface upon *Pth1r* deletion in MALPs (n=5-8; genotype effect calculated by two-way ANOVA; * $p < 0.05$, ** $p < 0.01$, *** $p < 0.001$, **** $p < 0.0001$ by Student's t-test).

C) Representative photomicrographs of endosteal TRAP+ osteoclasts (original magnification X400).

D) Representative photomicrographs of medullary/trabecular osteoclasts (original magnification X400).

D) Medullary/trabecular osteoclast number and surface showed a similar trend, albeit not significant (n=5-8; genotype effect calculated by two-way ANOVA).

F) Serum CTX and PINP concentrations were similar between the two groups (n=3-10; genotype effect calculated by two-way ANOVA).

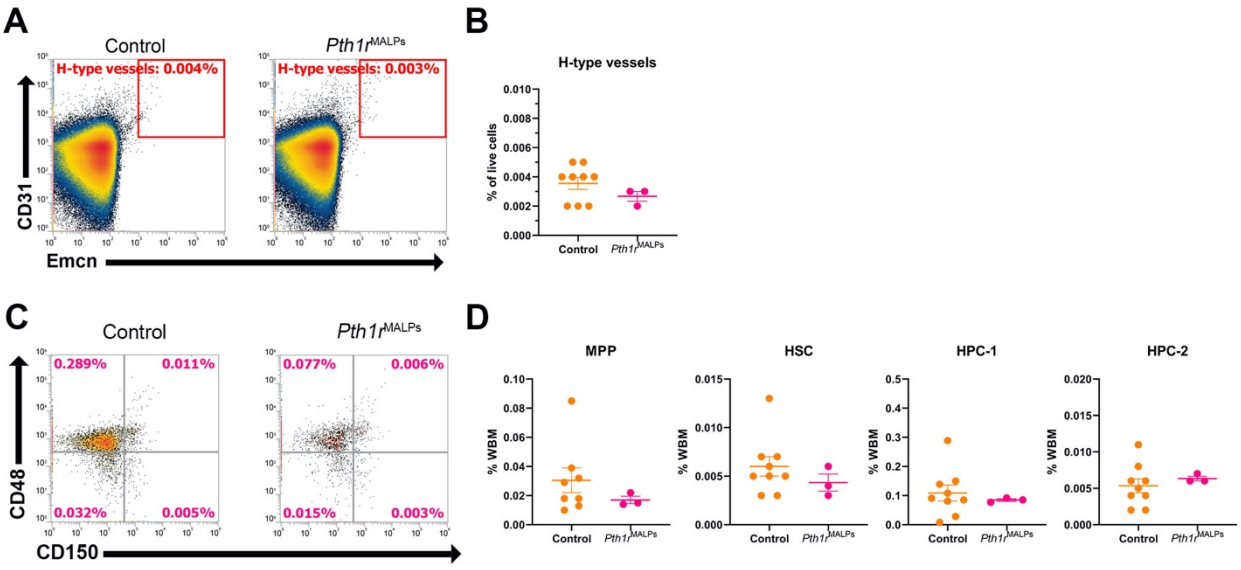

Figure 7: PTH signaling in MALPs is not crucial for their support for hematopoietic stem cells and type H endothelium.

A) Representative flow cytometry density plots of live CD31+Emcn+ cells (THECs) from flushed bone marrow from 4-week-old female mice.

B) Quantification of THECs. Control and *Pth1r*^{MALPs} mice had comparable percentages (n=3-9/group).

C) Representative flow cytometry density plots. Live cells were gated as Lineage-/Sca-1+/c-Kit+ (LSK cells). Quadrant 1: HPC-1, quadrant 2: HPC-2, quadrant 3: MPP, and quadrant 4: HSC.

D) Quantification of MPP, HSC, HPC-1, and HPC-2 reported as percentage whole bone marrow (WBM). Control and *Pth1r*^{MALPs} mice had similar proportions (n=3-8/group).

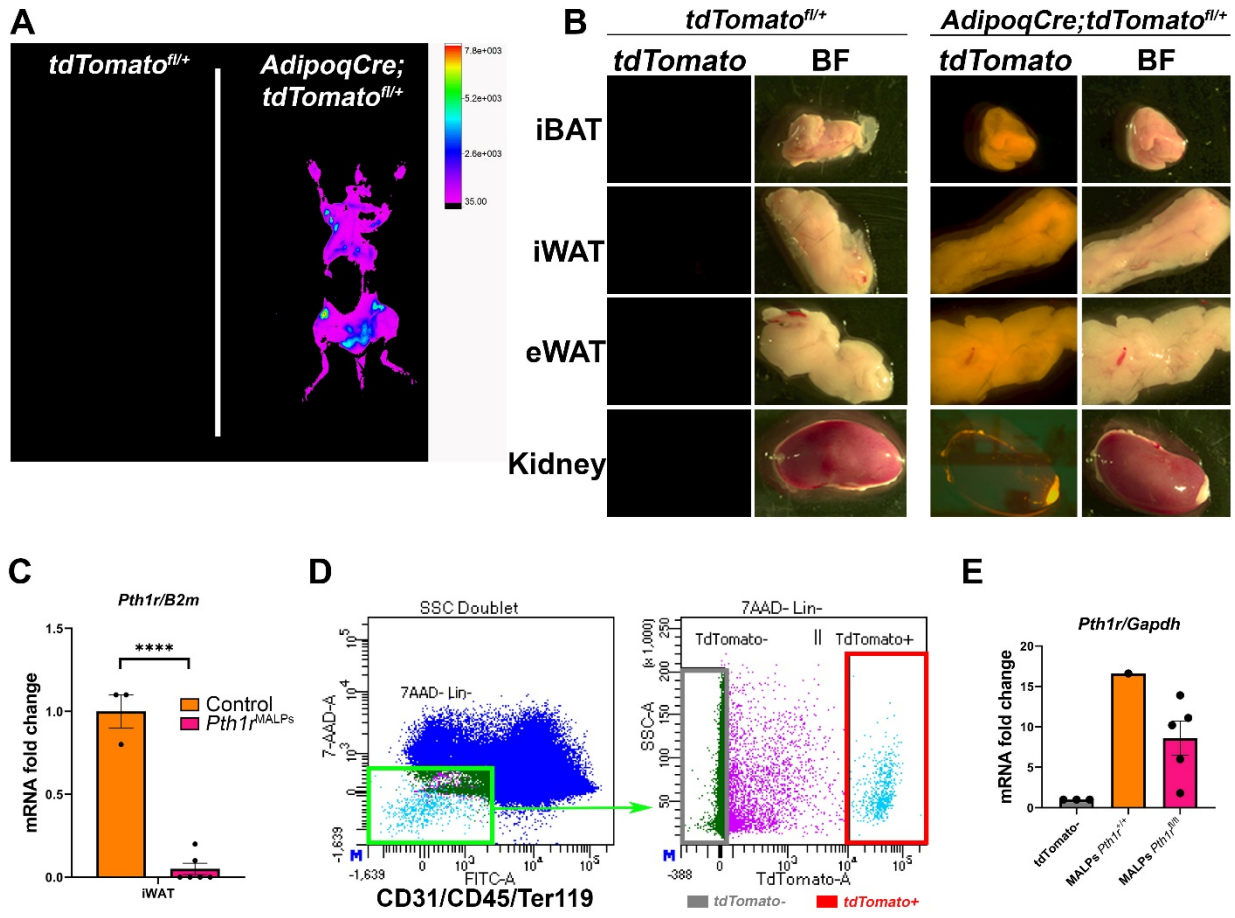

Figure S1: *AdipoqCre* targets the adipose lineage including MALPs.

A) Whole body florescent imaging of a *tdTomato*$^{fl/+}$ mouse (left) and *AdipoqCre;tdTomato*$^{fl/+}$ mouse (right) highlighting *tdTomato* expression in areas of adipose tissues.

B) Macroscopic images of peripheral adipose tissue and kidneys of *tdTomato*$^{fl/+}$ *AdipoqCre;tdTomato*$^{fl/+}$ mice. *tdTomato*$^{fl/+}$ mice lack *tdTomato* expression in all tissues examined. *AdipoqCre;tdTomato*$^{fl/+}$ mice express *tdTomato* only where *Adipoq* is expressed.

C) *Pth1r* gene expression from iWAT revealed 95% deletion of *Pth1r* (n=3-6/group, Student's t-test, **** $p < 0.0001$).

D) Gating strategy of flushed bone marrow cells. Singlets were gated as 7-AAD-/CD31-/CD45-/Ter119- and subsequently based on *tdTomato* positivity.

E) MALPs exhibit a 16-fold increase in *Pth1r* gene expression compared to *tdTomato*- cells. MALPs from *Pth1r*^{MALPs} mice exhibit a 50% decrease in *Pth1r* expression (n=1-5). BF; bright field, eWAT; epididymal white adipose tissue, iBAT; interscapular brown adipose tissue, iWAT; inguinal white adipose tissue.

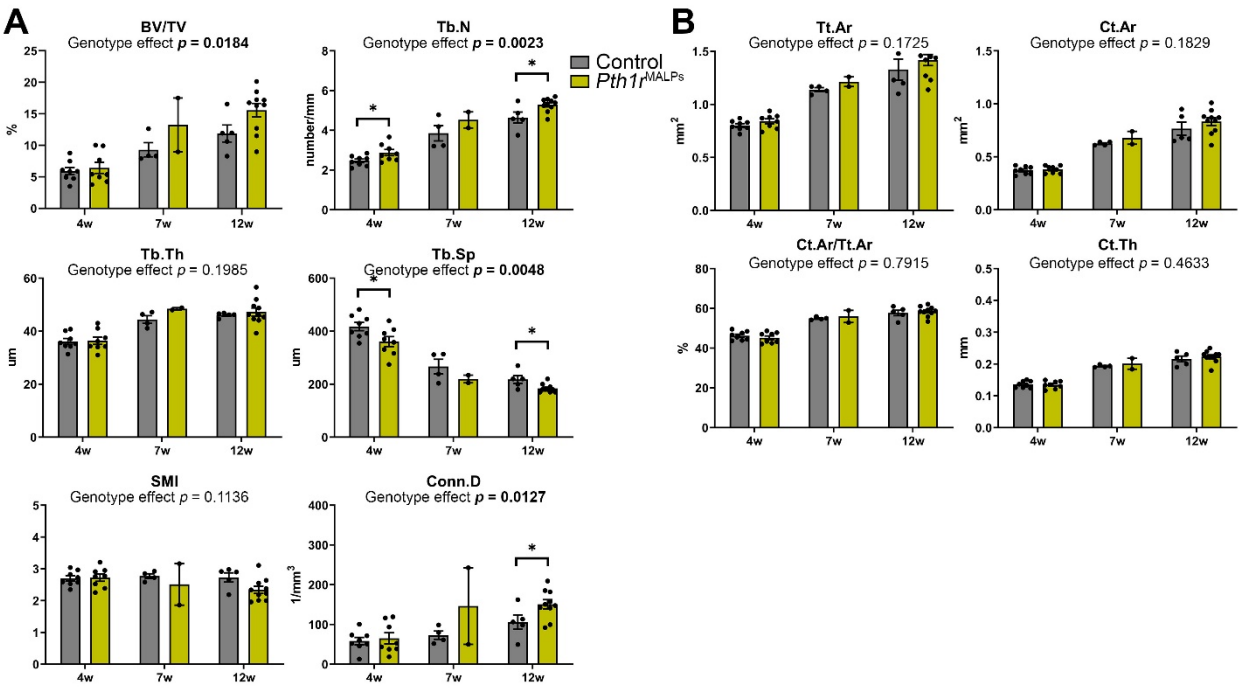

Figure S2: *Pth1r*^{MALPs} male mice exhibit a similar skeletal phenotype to *Pth1r*^{MALPs} female mice, albeit not significant.

A) µCT analysis of trabecular bone at 3 time points. *Pth1r*^{MALPs} male mice exhibited an increase in trabecular bone (n=2-11; genotype effect calculated by two-way ANOVA; * $p < 0.05$, ** $p < 0.01$, *** $p < 0.001$, **** $p < 0.0001$ by Student's t-test).

B) µCT analysis of cortical bone in mid-shaft tibia of *Pth1r*^{MALPs} male mice and littermate controls; no changes were observed between the two groups (n=2-11; genotype effect calculated by two-way ANOVA).

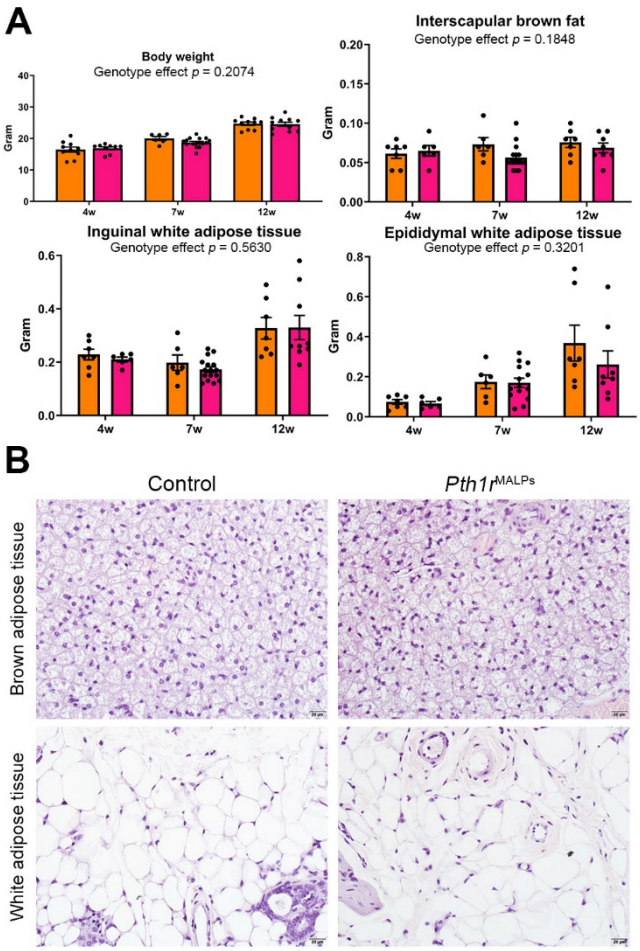

Figure S3: Ablation of *Pth1r* in adipose tissue does not alter peripheral adipose tissue.

A) Body weights and peripheral adipose tissue weights of *Pth1r*^{MALPs} mice and control littermates (n=5-16; genotype effect calculated by two-way ANOVA).

B) Photomicrographs of brown and white adipose tissues show similar adipocyte number and size in *Pth1r*^{MALPs} mice and control littermates.

Tables:

Table S1: Two-way ANOVA analysis of structural, dynamic, and cellular parameters.

	Two-way ANOVA		
Parameter	**Interaction**	**Age**	**Genotype**
BV/TV	0.6295	**0.0002**	**0.0010**
Tb.Th	0.1035	**< 0.0001**	0.1565
Tb.N	0.4836	**< 0.0001**	**< 0.0001**
Tb.Sp	0.9714	**< 0.0001**	**< 0.0001**
SMI	0.1683	**< 0.0001**	0.3856
Conn.D	0.1138	**< 0.0001**	**0.0200**
MAR	0.8533	**< 0.0001**	0.6878
MS/BS	0.0527	0.4878	**0.0066**
BFR/BS	**0.0368**	**< 0.0001**	0.0944
sL.S/BS	0.5281	**0.0001**	0.5203
dL.S/BS	0.0829	**0.0245**	**0.0429**
O.Th	0.3640	0.1921	0.3009
OS/BS	0.1455	**0.0196**	0.8077
N.Ob/B.Pm	0.0606	**0.0010**	0.8125
Ob.S/BS	0.0893	**0.0078**	0.7151

Abbreviations:

BV/TV, bone volume/tissue volume, Tb.Th, trabecular thickness, Tb.N, trabecular number, Tb.Sp, trabecular separation, SMI, structure model index, Conn.D, connectivity density, MAR, mineral apposition rate, MS/BS, mineralized surface/bone surface, BFR/BS, bone formation rate/bone surface, sL.S/BS, single label surface/bone surface,

dL.S/BS, double label surface/bone surface, O.Th, osteoid thickness, OS/BS, osteoid surface/bone surface, N.Ob/B.Pm, number of osteoblasts/bone perimeter, Ob.S/BS, osteoblast surface/bone surface

Table S2: Two-way ANOVA analysis of osmium-stained µCT analysis.

	Two-way ANOVA		
Parameter	**Interaction**	**Age**	**Genotype**
rBMAT density	**0.0120**	**<0.0001**	**0.0292**
rBMAT volume	**0.0069**	**<0.0001**	**0.0166**
cBMAT density	0.3529	**0.0052**	0.7787
cBMAT volume	0.4995	**0.0132**	0.7698

Abbreviations:

rBMAT, regulated bone marrow adipose tissue, cBMAT, constitutive bone marrow adipose tissue

Table S3: Two-way ANOVA analysis of osteoclast number and surface.

	Two-way ANOVA		
Parameter	**Interaction**	**Age**	**Genotype**
En N.Oc/B.Pm	0.5824	**0.0003**	**0.0017**
En Oc.S/B.Pm	0.8367	**0.0001**	**0.0012**
Med N.Oc/B.Pm	0.0508	0.2597	0.7071
Med Oc.S/B.Pm	**0.0161**	0.6171	0.8021

Abbreviations:

En, endosteal, Med, medullary, N.Oc/B.Pm, number of osteoclasts/bone perimeter, Oc.S/BS, osteoclast surface/bone surface

Flow cytometry and FACS antibodies table:

Antibody	Conjugate	Clone	Source	Catalog no.	Dilution
FACS antibodies					
Anti-CD45	FITC	30-F11	eBioscience	11-0451-82	1:100
Anti-Ter119	FITC	TER-119	BioLegend	116205	1:100
Anti-CD31	FITC	390	eBioscience	11-0311-82	1:50
Flow cytometry: MSC, OPC, and APC panel					
Anti-CD45	Super Bright 645	30-F11	eBioscience	64-0451-80	1:40
Anti-Ter119	Super Bright 645	TER-119	eBioscience	64-5921-82	1:40
Anti-CD31	Super Bright 645	390	eBioscience	64-0311-82	1:80
Anti-Sca-1	APC-Cy7	D7	BioLegend	108126	1:100
Anti-CD24	APC	M1/69	eBioscience	17-0242-82	1:200
Anti-Pdgfrα	Super Bright 436	APA5	eBioscience	62-1401-82	1:50
Flow cytometry: MPP, HSC, HPC-1, and HPC-2 panel					
Lineage cocktail	FITC	145-2C11; RB6-8C5; RA3-6B2;	BioLegend	133302	1:10

		Ter-119; M1/70			
Anti-Sca-1	APC-Cy7	D7	BioLegend	108126	1:100
Anti-CD117	APC	2B8	BioLegend	105811	1:50
Anti-CD150	eFluor 450	mShad150	eBioscience	48-1502-82	1:50
Anti-CD48	Super Bright 702	HM48-1	eBioscience	67-0481-82	1:50
Flow cytometry: Type-H endothelial cells					
Anti-CD31	Super Bright 645	390	eBioscience	64-0311-82	1:80
Anti-Endomucin	eFluor 660	eBioV.7C7 (V.7C7)	eBioscience	50-5851-82	1:100